AD-A068 558 GEORGE WASHINGTON UNIV WASHINGTON D C F/G 17/9
MAXIMUM ENTROPY SPECTRAL ANALYSIS IN THE SPATIAL DOMAIN.(U)
JUL 78 W R KING F30602-75-C-0121
UNCLASSIFIED RADC-TR-78-160 NL

| OF |
AD
A068558

END
DATE
FILMED
6-79
DDC

LEVEL II

AD A068558

RADC-TR-78-160
Phase Report
July 1978

MAXIMUM ENTROPY SPECTRAL ANALYSIS IN THE SPATIAL DOMAIN

William R. King

George Washington University

Approved for public release; distribution unlimited

DDC
RECEIVED
MAY 14 1979
D

ROME AIR DEVELOPMENT CENTER
Air Force Systems Command
Griffiss Air Force Base, New York 13441

79 05 11 074

This report has been reviewed by the RADC Information Office (OI) and is releasable to the National Technical Information Service (NTIS). At NTIS it will be releasable to the general public, including foreign nations.

RADC-TR-78-160 has been reviewed and is approved for publication.

APPROVED: Paul Van Etten

PAUL VAN ETTEN
Project Engineer

APPROVED: Joseph L Ryerson

JOSEPH L. RYERSON
Technical Director
Surveillance Division

FOR THE COMMANDER: John P. Huss

JOHN P. HUSS
Acting Chief, Plans Office

If your address has changed or if you wish to be removed from the RADC mailing list, or if the addressee is no longer employed by your organization, please notify RADC (OCTS) Griffiss AFB NY 13441. This will assist us in maintaining a current mailing list.

Do not return this copy. Retain or destroy.

MISSION
of
Rome Air Development Center

RADC plans and conducts research, exploratory and advanced development programs in command, control, and communications (C^3) activities, and in the C^3 areas of information sciences and intelligence. The principal technical mission areas are communications, electromagnetic guidance and control, surveillance of ground and aerospace objects, intelligence data collection and handling, information system technology, ionospheric propagation, solid state sciences, microwave physics and electronic reliability, maintainability and compatibility.

UNCLASSIFIED

SECURITY CLASSIFICATION OF THIS PAGE (When Data Entered)

REPORT DOCUMENTATION PAGE		READ INSTRUCTIONS BEFORE COMPLETING FORM
1. REPORT NUMBER RADC-TR-78-160	2. GOVT ACCESSION NO.	3. RECIPIENT'S CATALOG NUMBER
4. TITLE (and Subtitle) MAXIMUM ENTROPY SPECTRAL ANALYSIS IN THE SPATIAL DOMAIN		5. TYPE OF REPORT & PERIOD COVERED Phase Report June 1977 - December 1977
		6. PERFORMING ORG. REPORT NUMBER N/A
7. AUTHOR(s) William R. King		8. CONTRACT OR GRANT NUMBER(s) F30602-75-C-0121
9. PERFORMING ORGANIZATION NAME AND ADDRESS George Washington University Washington DC 20006		10. PROGRAM ELEMENT, PROJECT, TASK AREA & WORK UNIT NUMBERS 61101F 450611P0
11. CONTROLLING OFFICE NAME AND ADDRESS Rome Air Development Center (OCTS) Griffiss AFB NY 13441		12. REPORT DATE July 1978
		13. NUMBER OF PAGES 71
14. MONITORING AGENCY NAME & ADDRESS(if different from Controlling Office) Same		15. SECURITY CLASS. (of this report) UNCLASSIFIED
		15a. DECLASSIFICATION/DOWNGRADING SCHEDULE N/A

16. DISTRIBUTION STATEMENT (of this Report)

Approved for public release; distribution unlimited.

17. DISTRIBUTION STATEMENT (of the abstract entered in Block 20, if different from Report)

Same

18. SUPPLEMENTARY NOTES

RADC Project Engineer: Paul VanEtten (OCTS)

19. KEY WORDS (Continue on reverse side if necessary and identify by block number)

Maximum Entropy Method
Antennas
Super Angular Resolution

20. ABSTRACT (Continue on reverse side if necessary and identify by block number)

Desirable antenna pattern characteristics include high resolution, accurate angular prediction, peak detection at low (S/n) levels, and stability under noisy conditions and multiple target environments. In this necessarily encompassing and cursory investigation, antenna patterns computed using MESA have exhibited these desirable properties to a relatively high degree of measure.

Resolution with MESA is exceptional even under noisy conditions and in multiple and mixed target environments. High resolution is maintained even at

DD FORM 1 JAN 73 1473 EDITION OF 1 NOV 65 IS OBSOLETE

UNCLASSIFIED

SECURITY CLASSIFICATION OF THIS PAGE (When Data Entered)

very large angles of incidence. Estimates of signal angle appear to be quite accurate even under difficult signal conditions, and peak detection with MESA is obviously better than that provided by the Fourier transform. However, it is perhaps most significant that MESA exhibits good stability properties with use of the optimal filter size.

Non-zero signal phase does apparently affect signal levels and consequently signal detectability in an adverse manner, although averaging over many antenna patterns does help to restore the affected signal levels. The problem of peak splitting is apparently avoided although not corrected with use of an optimal filter order.

It can only be concluded that MESA is a most promising signal processing technique as it appears to provide significant improvements over conventional techniques for processing phased array antenna data. While the results of this investigation demonstrate that MESA may be used to obtain very desirable antenna patterns, MESA characteristics are not defined in a precise manner. Hopefully, further investigations will establish MESA characteristics in a more definitive manner.

When new techniques provide significant improvements in certain characteristics, it is always suspected that other characteristics are degraded. Of course, usually such suspicions are well founded. However, the Maximum Entropy Spectral Analysis technique developed by Burg appears to have withstood most of the usual criticisms.

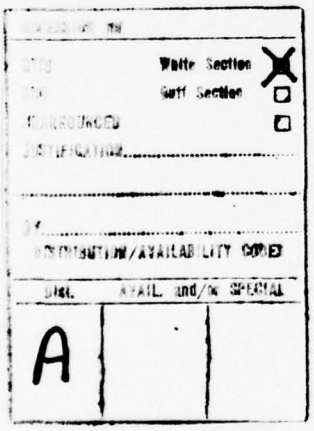

TABLE OF CONTENTS

LIST OF ILLUSTRATIONS

Introduction

In recent years several methods have been introduced for estimating power spectra with considerably greater resolution than that provided by the conventional periodogram or the Blackman-Tukey windowed Fourier transform. Included among such techniques are maximum entropy spectral analysis (MEASA) introduced by Burg (1967), autoregressive model (AR) spectral estimation introduced by Parzen (1968), and the method of maximum likelihood as demonstrated by Capon (1969). Other methods offering high resolution, which utilize the Fourier transform, are described by Gerchburg (1974) and Papoulis (1975). And more recently another spectral estimator has been introduced by Gray (1977).

While none of these spectral estimators have been thoroughly investigated, there have been a few comparative examinations of some of the techniques conducted by Lacoss (1971), Ulrych and Bishop (1975), and Nuttall (1976). Of the comparisons investigated, in general, superior results are achieved using the MESA method and the Burg technique (Burg, 1968) for estimating filter coefficients. The results are dramatic, and suggest that investigations of MESA and other high resolution techniques be continued. Because of the high resolution and stability achieved with MESA in such initial investigations, these same properties are investigated further in this report where MESA is applied to the analysis of simulated, multichannel, spatial, phased-array data.

In the initial paper by Burg (1967), where the principle of maximum entropy spectral analysis is first suggested, the prediction error filter coefficients (which maximize the entropy) are specified with knowledge of the autocorrelation coefficients. However, in a second MESA paper, Burg (1968) defined the prediction error filter coefficients as a function of a set of uniformly spaced data samples representative of the function of interest. In addition, Burg simplified the method for obtaining the filter coefficients with use of Levinson's recursion equations, and also noted in the second paper that the mean squared prediction errors may be minimized in both the forward and backward directions. These suggestions served to greatly facilitate the implementation of MESA and to significantly enhance the MESA properties. Taken together, the improvements suggested by Burg (1968) are often referred to as the "Burg technique."

The concept of estimating power spectra by maximizing entropy appears unique in the history of science, yet the resultant expression for power spectra is identical to the representation of the all pole method or autoregressive model (AR) introduced by Parzen (1968). In fact, van den Bos (1971) and Kaveh and Cooper (1976) have noted that MESA, as outlined by Burg (1967), is equivalent to the AR method as described by Parzen. Therefore, it is of consequence to note that the different spectral estimates sometimes predicted with the two spectral estimation methods are not due to inherent model differences, but rather, are due to the different methods used for evaluating the corresponding filter coefficients. With this realization, Ulrych and Bishop (1975) conducted a comparative anlalysis of the Burg and Yule-Walker (Yule, 1927; Walker, 1931) techniques for evaluating MESA and AR filter coefficients. In a comparison of spectral estimation of

harmonic components, Ulrych and Bishop showed that the MESA-Burg technique provided significantly greater resolution than did the AR-Yule-Walker technique. Ulrych and Bishop noted that the resolution differences are not surprising when it is realized that the Yule-Walker has assumed a zero extension of the data samples; whereas the Burg technique contains no assumptions concerning the non-sampled data field.

Since the MESA and AR methods are most significant when processing short data sets, it is natural to utilize such methods for processing data collected with multi-element electromagnetic antennas or acoustical arrays. For with use of such methods it may well be possible to achieve high resolution using unusually short antenna array. Consequently, in this report, the resolution property of the MESA-Burg technique is examined as a function of input signal-to-noise (S/N) ratios, number of antenna elements, numbers of signals, incident signal angle, relative signal amplitudes, and relative signal phase.

THEORY

SECTION II

Theory

The maximum entropy power spectra (MESA), which was introduced by Burg (1967), has been derived by Parzen (1969) using statistical methods, and by van den Bos (1971) using an all pole model representation. In order to further the understanding and acceptance of MESA, another derivation suggested by Blizard (1977) is presented based upon discrete convolution filtering and minimization of the mean squared error.

Consider the one step discrete convolution prediction filter described by Levinson (1947) as follows:

$$\hat{x}_t = \sum_{n=1}^{N} a_n x_{t-n} \tag{1}$$

where $\hat{x}_t$ is the prediction at time t of the function x_t which is sampled at time intervals, $n\Delta t$, and the N prediction coefficients are given by $a_1, a_2, \ldots a_N$. The error of the one step prediction is ε_t given as follows:

$$\varepsilon_t = x_t - \hat{x}_t$$

$$\varepsilon_t = x_t - \sum_{n=1}^{N} a_n x_{t-n} \tag{2}$$

The filtering and error analysis represented by Eqs. (1) and (2) is illustrated in Fig. (1) where filter coefficients a_n are multiplied by values of x_t sampled at time intervals of $n(\Delta t)$, and resultant multiplications are summed to obtain the prediction $\hat{x}_t$. The predicted signal $\hat{x}_t$

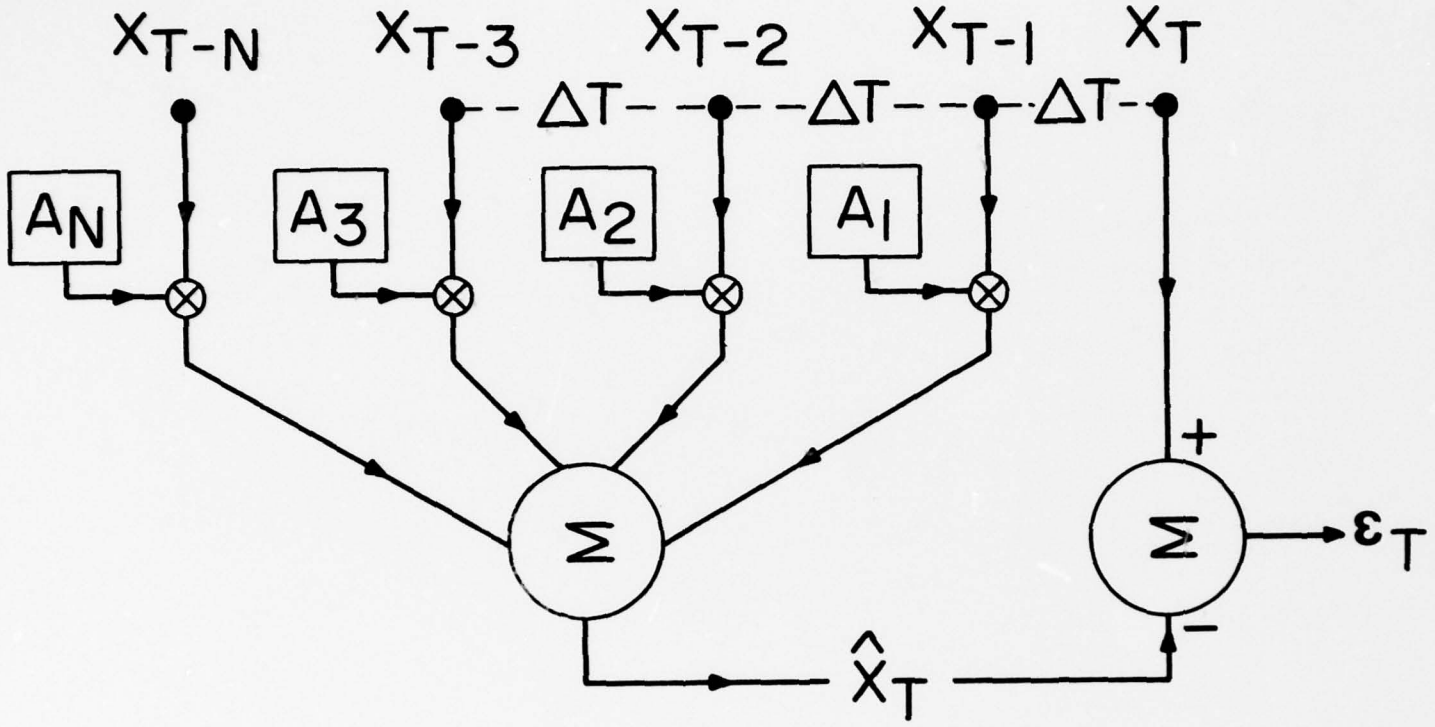

PREDICTION ERROR FILTER

FIG. 1

and the actual signal x_t are subsequently substracted to obtain the prediction error ε_t.

For convenience the prediction error filter γ is introduced as follows:

$$\varepsilon_t = \sum_{n=0}^{N} \gamma_n \, x_{t-n} \tag{3}$$

where in comparing Eq. (2) and (3), it is observed that

$$\gamma_0 = 1 \; ; \; \gamma_n = -a_n, \; n \geq 1$$

Equation (3) is transformed to frequency space with the Fourier transform to obtain the following equation:

$$\xi_N(\omega) = X(\omega) \sum_{n=0}^{N} \gamma_n \, e^{i\omega n(\Delta t)} \tag{4}$$

where it is noted that the Fourier transform of a function delayed $n(\Delta t)$ units is the exponential

$$e^{i\omega n(\Delta t)}$$

multiplied by the transformed function. The power spectra density function $P(\omega)$ is defined as follows:

$$P(\omega) = X^2(\omega)/W$$

where W is the bandwidth defined by the sampling interval Δt,

$$W = \frac{1}{(\Delta t)}$$

If the signal distribution function $X(\omega)$ is given by Eq. (4), the power spectra density function becomes as follows:

$$P(\omega) = \frac{\xi_N^2(\omega)/W}{\left| \sum_{n=o}^{N} \gamma_n \; e^{i\omega n(\Delta t)} \right|^2} \tag{5}$$

$$P(\omega) = \frac{P_N/W}{\left| 1 + \sum_{n=1}^{N} \gamma_n \; e^{i\omega n(\Delta t)} \right|^2} \tag{6}$$

where the error power $\xi_N^2(\omega)$ is represented by P_N. A requirement that the spectral error power $\xi_N^2(\omega)$ be a minimum results in P_N being independent of frequency as follows:

$$\frac{d\xi_N^2(\omega)}{d\omega} = 0$$

$$\xi_N^2(\omega) = \text{constant} \tag{7}$$

$$P_N = \text{constant}$$

It follows that if P_N is a constant then the prediction error filter γ is a whitening filter, and P_N is also the mean of the total squared error as follows:

$$P_N = \xi_N^2(\omega)$$

$$P_N = \frac{1}{W}\left[\xi_N^2(\omega)W\right] \tag{8}$$

The power spectra density function $P(\omega)$ given by Eq. (6) is the same MESA equation introduced by Burg (1967) and later derived with detailed steps by Barnard (1975).

The power spectra density (Eq. 6) may also be expressed as a wavenumber power spectra density as follows:

$$P(k) = \frac{P_N/k_{max}}{\left| 1 + \sum_{n=1}^{N} \gamma_n \; e^{ikn(\Delta x)} \right|^2} \tag{9}$$

where the time (t) and frequency (f) variables have been transformed to space and wavenumber variables using the following relations:

$$\omega = kc, \qquad \Delta t = \Delta x/c$$

for $k = (2\pi/\lambda) \cos\theta$

λ = signal wavelength

θ = signal angle of incidence

c = signal velocity

k_{max} = wavenumber bandwidth $= 2\pi/\lambda$

Utilization of the MESA power spectra equation (Eqs. 6 and 9) requires that the prediction error coefficients γ_n and the mean error power P_N be known. These unknown parameters may be specified by minimizing the average time dependent prediction error power, $\overline{\varepsilon_t^2}$. The resulting N + 1 equations, which are derived in Appendix A, are presented in a matrix formulation as follows:

$$\begin{bmatrix} r_o & r_1 & r_2 & r_3 & \cdots & r_N \\ r_1 & r_o & r_1 & r_2 & \cdots & r_{N-1} \\ r_2 & r_1 & r_o & r_1 & \cdots & r_{N-2} \\ \cdot & & & & & \\ \cdot & & & & & \\ \cdot & & & & & \\ r_N & r_{N-1} & r_{N-2} & r_{N-3} & \cdots & r_o \end{bmatrix} \begin{bmatrix} \gamma_1 \\ \gamma_2 \\ \gamma_3 \\ \cdot \\ \cdot \\ \cdot \\ \gamma_N \end{bmatrix} = \begin{bmatrix} P_N \\ 0 \\ 0 \\ \cdot \\ \cdot \\ \cdot \\ 0 \end{bmatrix} \tag{10}$$

where it is known that $\gamma_1 = 1$, and it is assumed that the autocorrelation coefficients r_i (with lag $i\Delta t$) are known for N lags.

The autocorrelation coefficients have the following definition:

$$r_n = \lim_{M\to\infty} \frac{1}{2M+1} \sum_{k=-M}^{M} X_k X_{k-n} \tag{11}$$

But for a finite data set, the autocorrelation coefficients may be computed by approximating Eq. (11) with a finite summation over M data samples.

For large sized filters (N large) solution of the N+1 equations given by Eq. (10) becomes very tedious. Fortunately, Burg (1968) demonstrated a more expeditious method for specifying the unknown prediction error coefficients which appear in Eqs. (6) and (9). Burg noted that the unknown parameters P_N and γ_n^N may be evaluated with repeated use of Levinson's recursion relations,

$$P_{N+1} = P_N \left[1 - (\gamma_{N+1}^{N+1})^2\right] \tag{12}$$

$$\gamma_n^{N+1} = \gamma_n^N + \gamma_{N+1}^{N+1} \gamma_{N-n+2}^N \tag{13}$$

for $P_1 = r_o^2$,

$$\gamma_1^{N+1} = 1 \text{ and } N \geq 1$$

and with knowledge of γ_{N+1}^{N+1}, which is shown in Appendix B to have the following representation.

$$\gamma_{N+1}^{N+1} = \frac{2\sum_{k=1}^{M=N-1} \beta_k^N \alpha_{k+n}^N}{\sum_{k=1}^{M=N-1} \left[(\beta_k^N)^2 + (\alpha_{k+N}^N)^2\right]} \tag{14}$$

where the forward prediction error is α_k^N and the backward prediction error is β_k^N. The three equations, Eq. (12), (13), and (14), comprise the Burg technique as originally demonstrated by Burg (1968) and later generalized in detail by Anderson (1974) and Barnard (1975).

The remainder of this report is concerned with the properties exhibited by the MESA wavenumber power spectra equation (Eq. 9) when evaluated using the Burg technique given by Eqs. 12-14.

Signal Simulation

Resolution properties of the MESA-Burg technique are examined using simulated antenna data. Input signals to a linear (line), multi-element, phased-array antenna are assumed to be plane waves mixed with white, Guassian noise. The multi-channel signals are pre-processed with narrow band filtering and channel delays which serve to "direct" (or steer) the antenna in the direction of the incident plane wave signal. The pre-processing methods are illustrated in Fig. (2) where the nth channel is depicted as delayed (n-1) Δt seconds for

$$\Delta t = \Delta x \sin(\theta) / c$$

where c is the velocity of the incident signal, Δx is the antenna element spacing and θ is the look angle of the steered array measured relative to the normal to the array.

The incident signal $x_n(\theta)$ to the n^{th} antenna element is represented as follows:

$$x_n(\theta) = A \cos\left[\Omega_n(\theta) + Q_n\right] \tag{15}$$

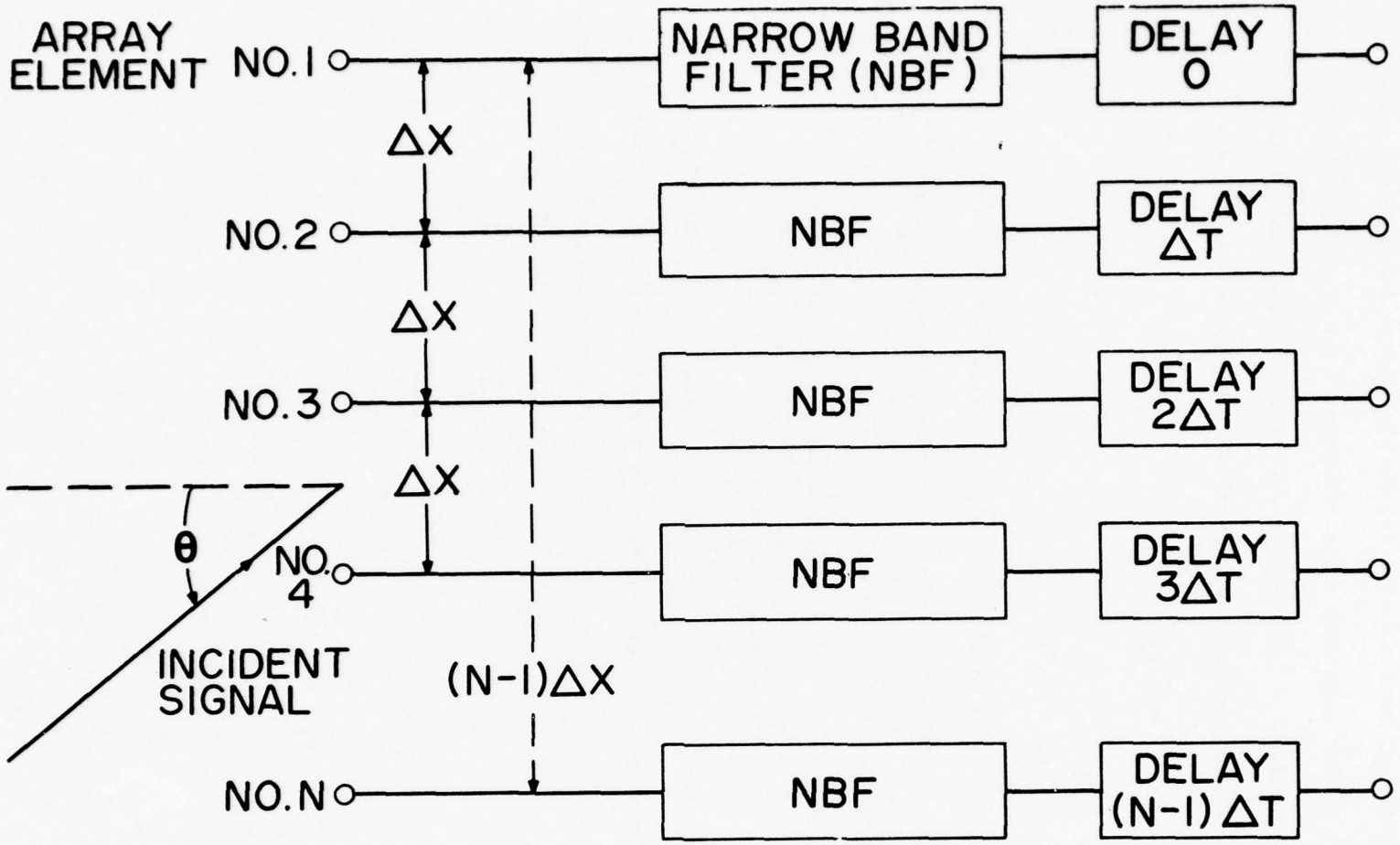

PREPROCESSING OF A LINEAR PHASED ARRAY

FIG. 2

where A is the signal amplitude, $\Omega_n(\theta)$ is the signal total phase, and Q_n is a random number representative of Gaussian noise. The amplitudes A and Q_n are relative, and are determined by a Gaussian distribution with variance σ^2 and a specified signal-to-noise ratio as follows:

$$\frac{S}{\eta} = \frac{A^2}{2\sigma^2} \tag{16}$$

$$q_n = e^{-Q_n^2/2\sigma^2} \tag{17}$$

where (S/η) is the input signal-to-noise power ration, $2\sigma^2$ is the average noise power, and q_n is a random number between 0 and 1.0 obtained using a "white" random number generator.

The signal phase $\Omega_n(\theta)$ has three components as follows:

$$\Omega_n(\theta) = 2\pi \left[n-1\right] \cdot \left[\Delta x/\lambda\right] \cdot \left[\sin(\theta) - \sin(\theta_s)\right] - \phi \tag{18}$$

where θ is the array look angle, θ_s is the angle of the incident signal relative to the normal to the array, ϕ is the incident signal initial phase with values between 0 and 2π , and λ is the signal wavelength given by

$$\lambda = c/f$$

For all signals analyzed in this report the ratio $(\Delta x/\lambda)$ has the value 0.5; i.e.:

$$\Delta x/\lambda = 0.5$$

In conventional beamforming all N antenna elements are summed such that the total $\mathbf{X}(\theta)$ is the following summation:

$$\mathbf{X}(\theta) = \sum_{n=1}^{N} \{A \cos\left[\Omega_n(\theta)\right] + Q_n\} \tag{19}$$

and the conventional antenna power pattern is computed in units of decibels as follows:

$$dB = 10 \text{ Log } \left[\mathbf{X}^2 (\theta) / \mathbf{X}^2 (\theta_s) \right] \tag{20}$$

However the MESA technique requires multi-channel data which is given by Eqs. (15) and (18).

Conventional antenna patterns are compared with MESA patterns whenever such comparisons are considered worthwhile. It is specifically noted that the signal-to-noise (S/η) is defined at the antenna element and is the same for each antenna element. Consequently, the signal-to-noise ratio does not include the conventional antenna gain factor.

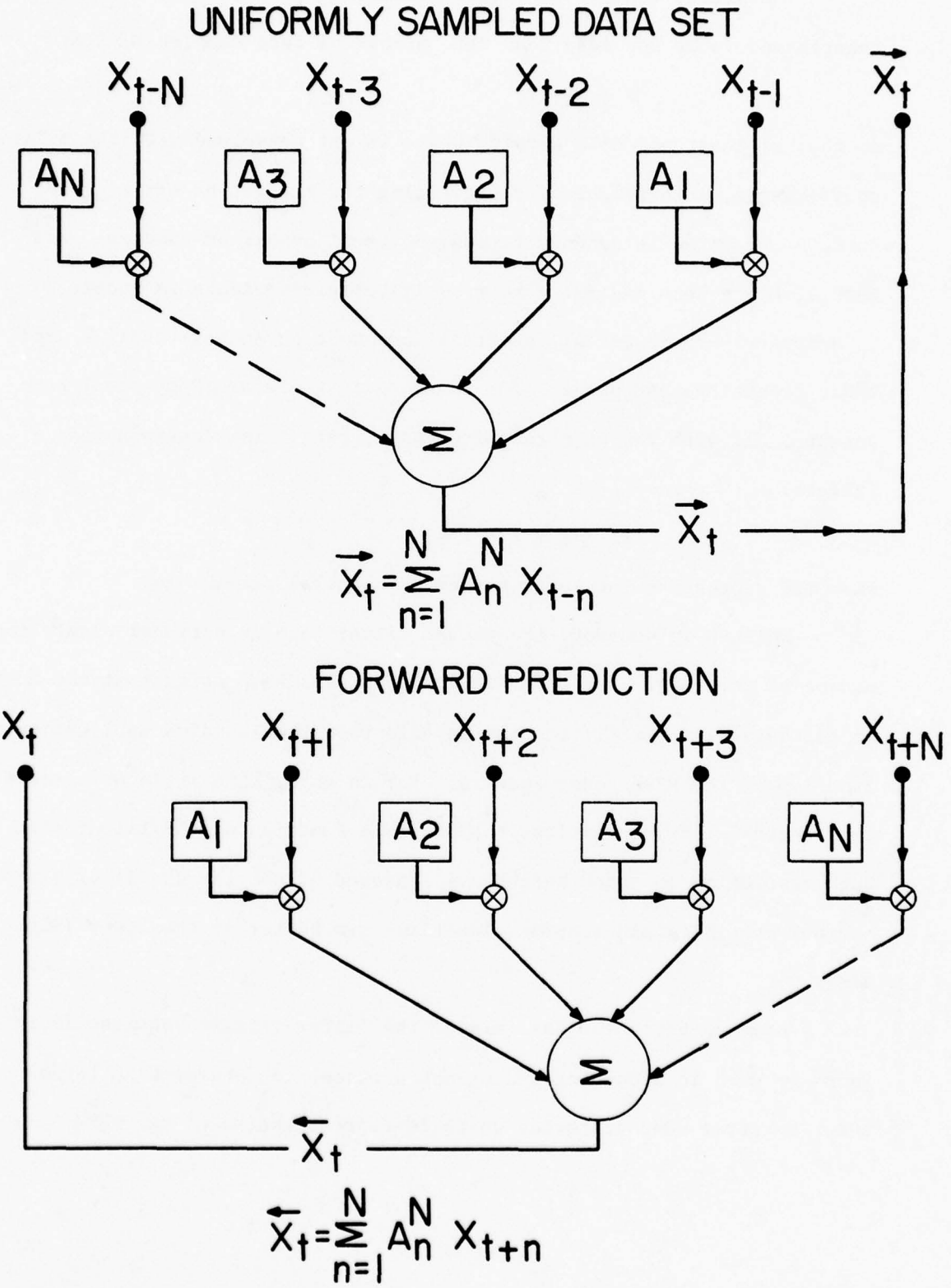
UNIFORMLY SAMPLED DATA SET
X_{t-N}
X_{t-3}
X_{t-2}
X_{t-1}
$\vec{X}_t$
A_N
A_3
A_2
A_1
Σ
$\vec{X}_t$
$\vec{X}_t = \sum_{n=1}^{N} A_n^N X_{t-n}$
FORWARD PREDICTION
X_t
X_{t+1}
X_{t+2}
X_{t+3}
X_{t+N}
A_1
A_2
A_3
A_N
Σ
$\overleftarrow{X}_t$
$\overleftarrow{X}_t = \sum_{n=1}^{N} A_n^N X_{t+n}$
BACKWARD PREDICTION

FIG. 3

Optimal Filter Size

The size N (number of filter coefficients) of a MESA filter is constrained to be one less than the number of data samples M, i.e.

$$N \leq M - 1$$

so that at least one data sample, which is not convolved with the filter coefficients, is available for estimating the prediction error. The lower bound on N is dependent upon the total number of spectral parameters, since some minimal number of filter coefficients is required to accurately represent all spectral component parameters such as amplitude, frequency, and phase. For instance if there are P spectral components, all with the same relative phase, then N is constrained as follows:

$$2P \leq N \leq M - 1 \tag{21}$$

where 2P represents the total number of spectral parameters.

While N is bounded, the actual filter size is optional within the bounds of Eq. (21). Anderson (1974) and others have noted that the criteria for selecting the filter size depends upon the intended application or function of the MESA power spectra. For in using MESA it is observed that the spectral characteristics of MESA are a function of the filter size. Both resolution and peak height are improved at the larger filter sizes, whereas stability and accuracy sometimes are better at the lower filter sizes.

Some criteria for determining the filter size is required if MESA is to be used in a completely automated manner to determine an unknown power spectra. One criteria, which is representative of two MESA

characteristics is the output signal-to-noise power ratio. Both peak height and resolution are two inter-related properties that are optimal with maximization of the output signal-to-noise (S/η) power ratio. King (1977) has noted that maximization of the output (S/η) power ratio at a spectral peak is a reliable criteria. Another criteria developed by Akaike (1970) has been investigated by Ulrych and Bishop (1975) and found to be only partially satisfactory.

King (1977) noted that the output (S/η) power ratio at a spectral peak ω_o is given by

$$(S/\eta)_{\omega_o} = \frac{P(\omega_o)}{P_N} \tag{22}$$

where the power spectra is evaluated at the spectral peak ω_o. With use of the power spectra expression (Eq. 6),

$$\left(\frac{S}{\eta}\right)_{\omega_o} = \frac{1}{\Gamma_N^2(\omega_o)} \tag{23}$$

where

$$\Gamma_N^2(\omega_o) = W \left| 1 + \sum_{n=1}^{N} \gamma_n e^{i\omega_o n(\Delta t)} \right|^2 \tag{24}$$

A maximum $(S/\eta)_{\omega_o}$ requires that $\Gamma_N(\omega_o)$ be a minimum. Therefore, an optimal filter size is the filter size (N_o) that minimizes $\Gamma_N(\omega o)$.

If the maximum (S/η) ratio is a criteria for determining the filter size, then the MESA properties of accuracy and stability are not optimized, and remain as inherent MESA characteristics. Both accuracy and stability (under varying noise fields) have been satisfactory with use of a maximum (S/η) output. However, when signal relative phase is non-zero, spectral peaks of the computed power spectra are often instable. Sometimes averaging

of such computed spectra appears to restore the stability. Examples of MESA antenna patterns of phase shifted signals are provided in a subsequent section.

Of course, maximization of the output (S/η) at each spectral peak requires that the peak locations ω_o be known. The peak locations may be determined by solving for the roots of the function $\dot{r}(\omega)$ at a stable and accurate low order filter size.

An example of the value of maximizing the output $(S/\eta)_{\omega_o}$ is given in Fig. (4a)-(4g) where the MESA wavenumber spectra is computed for a signal located at 0^o (broadside to the antenna). The antenna has 8 elements and the input signal-to-noise ratio is 10 dB per element. The MESA power spectra are shown computed for all possible filter sizes.

$$2 \leq N \leq 7$$

in fig. (4a) - (4f).

A common problem with MESA, line splitting is noticed to occur at the large filter sizes $5 \leq N \leq 7$. At the lower filter sizes $2 \leq N \leq 4$, the power spectra having the best resolution and greatest peak height occurs at the filter size N=4, Fig. (4c). The filter size, N=4, is also the filter size determined by maximizing the output $(S/\eta)_{\omega_o}$ ratio, and the optimal power spectra for N=4 is shown in Fig. (4g). Of the six possible filter sizes, the power spectra for N=4 is clearly the power spectra with the best resolution and peak height. Maximization of the output $(S/\eta)_{\omega_o}$ also serves to avoid such problems as line splitting as observed with the example given.

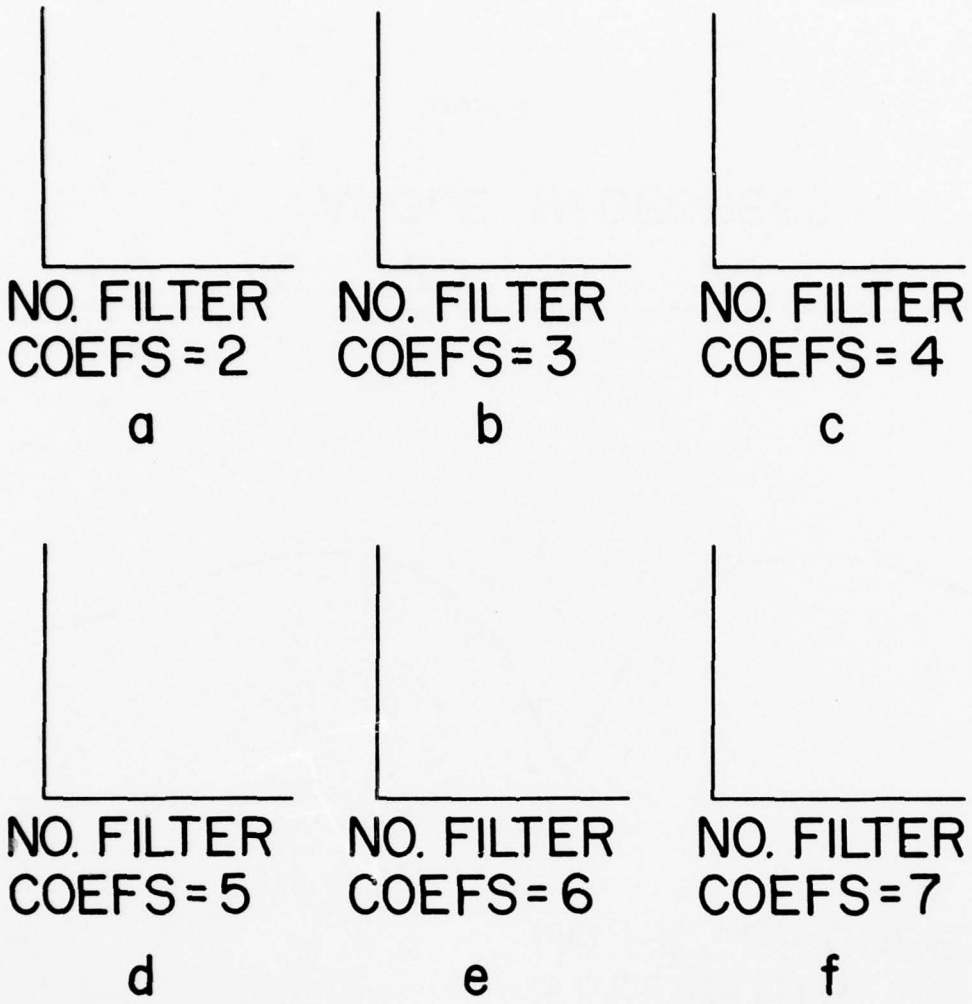

FILTER SIZES

FIG. 4a-4g

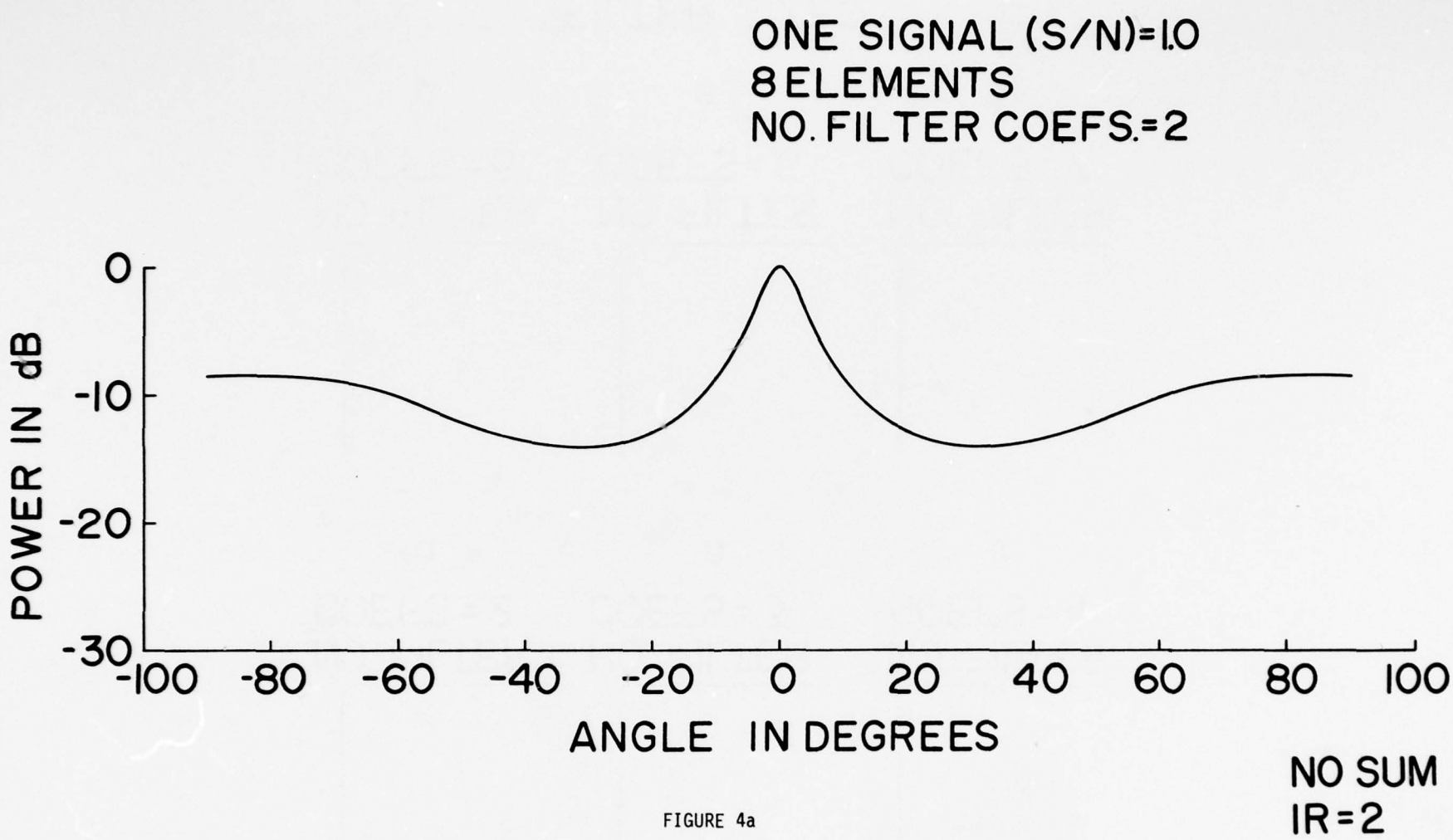
ONE SIGNAL (S/N)=1.0
8 ELEMENTS
NO. FILTER COEFS.=2
POWER IN dB
0
-10
-20
-30
-100
-80
-60
-40
-20
0
20
40
60
80
100
ANGLE IN DEGREES
NO SUM
IR=2

FIGURE 4a

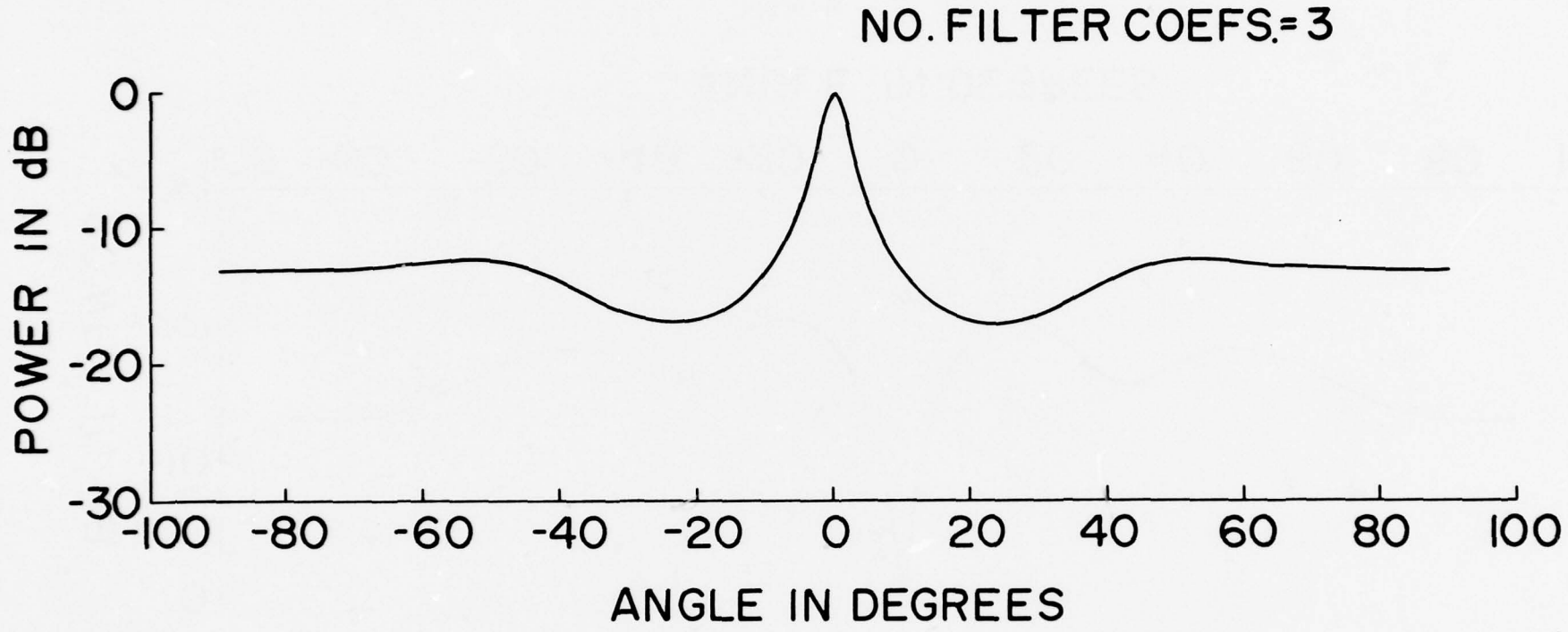
NO. FILTER COEFS.= 3
POWER IN dB
0
-10
-20
-30
-100
-80
-60
-40
-20
0
20
40
60
80
100
ANGLE IN DEGREES

FIGURE 4b

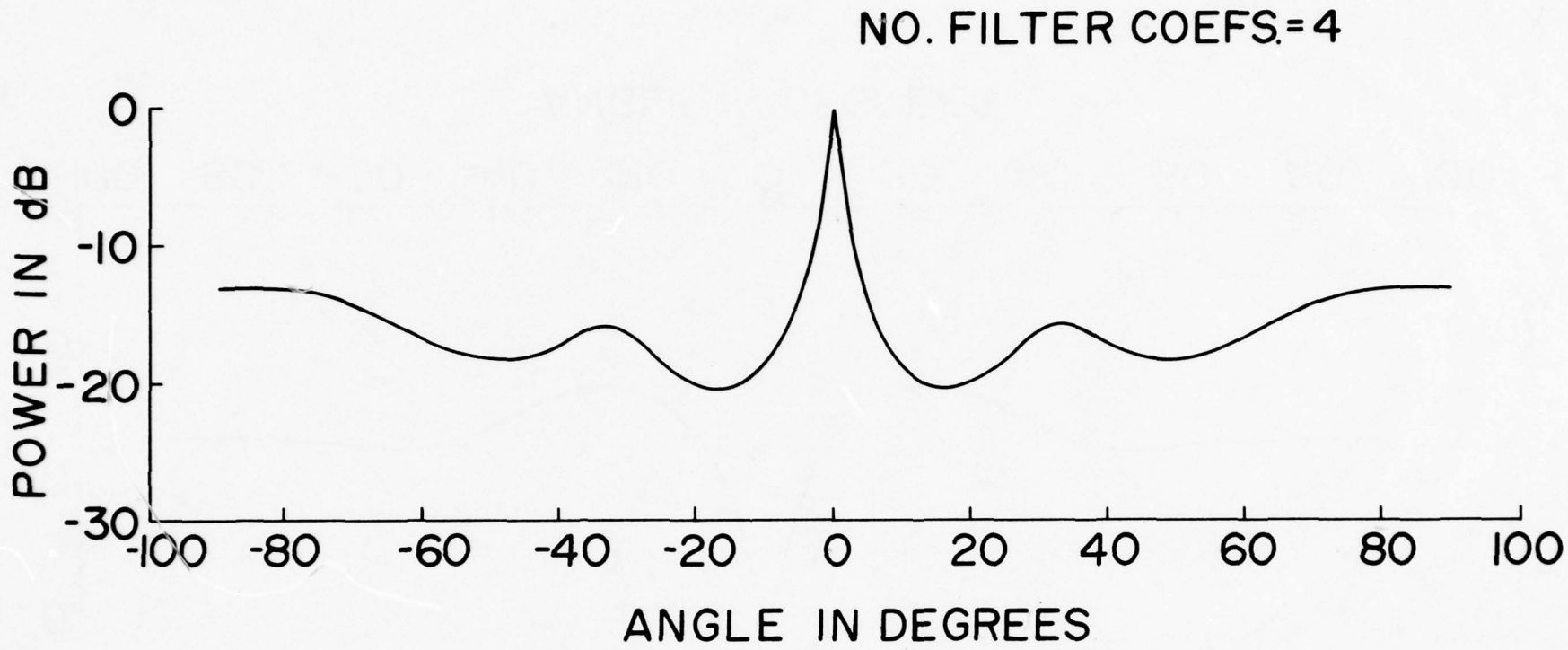
NO. FILTER COEFS.=4
POWER IN dB
0
-10
-20
-30
-100
-80
-60
-40
-20
0
20
40
60
80
100
ANGLE IN DEGREES

FIGURE 4c

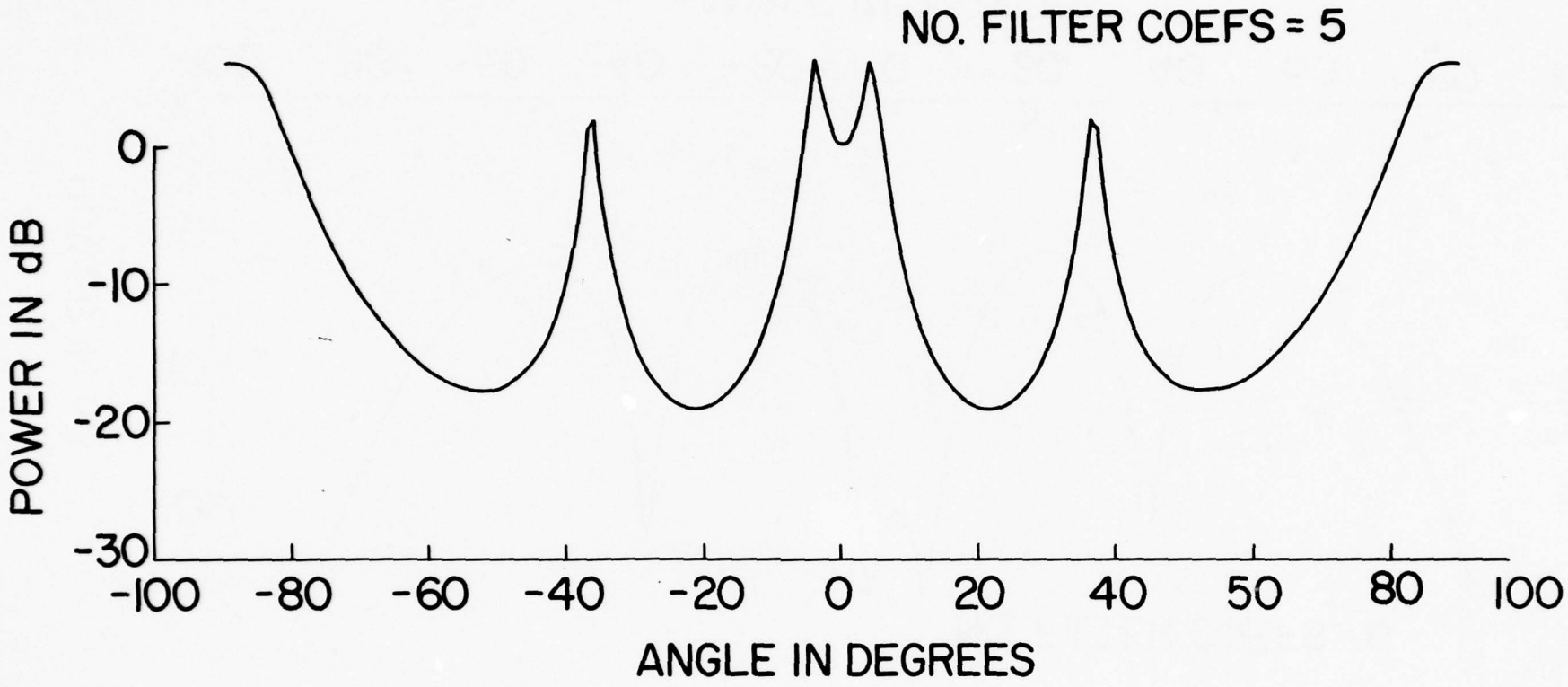
NO. FILTER COEFS = 5
POWER IN dB
0
-10
-20
-30
-100
-80
-60
-40
-20
0
20
40
50
80
100
ANGLE IN DEGREES

FIGURE 4d

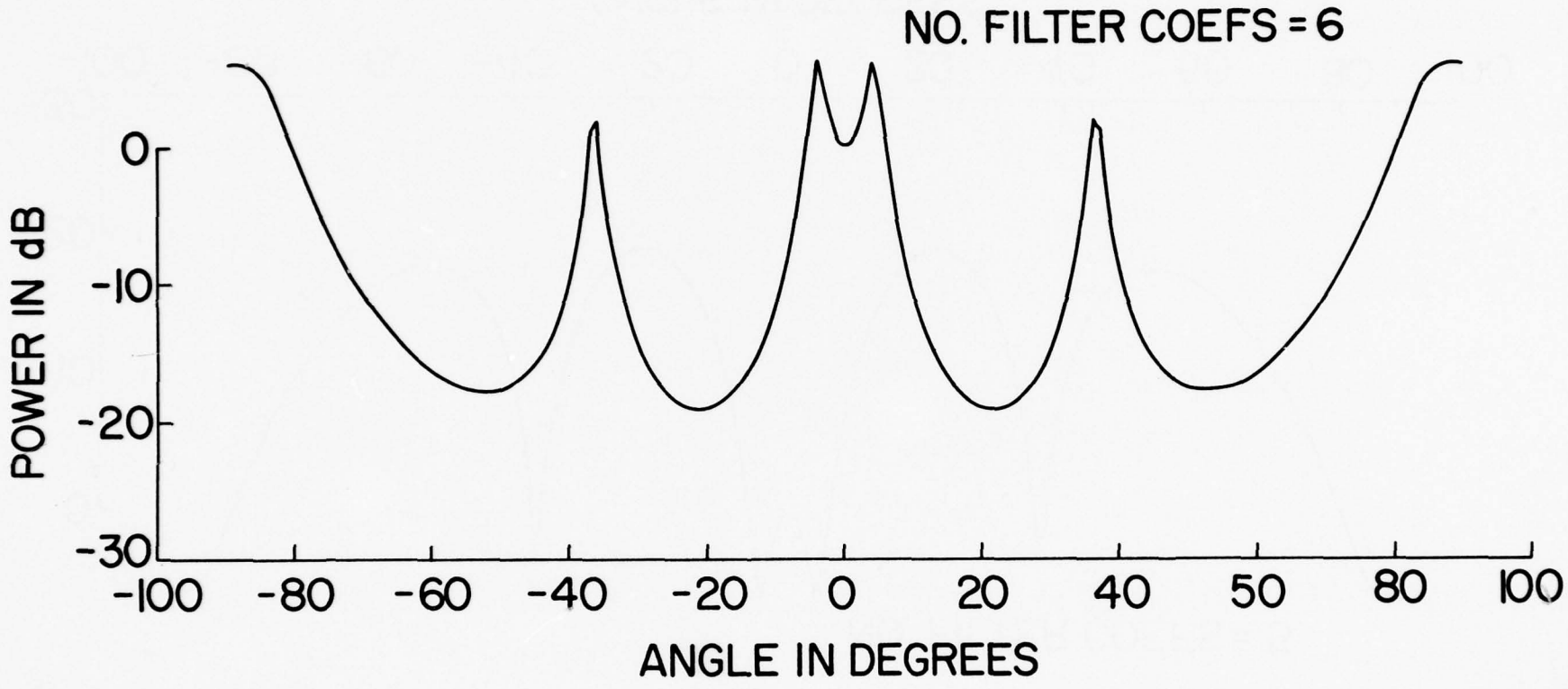
NO. FILTER COEFS = 6
POWER IN dB
0
-10
-20
-30
-100
-80
-60
-40
-20
0
20
40
50
80
100
ANGLE IN DEGREES

FIGURE 4e

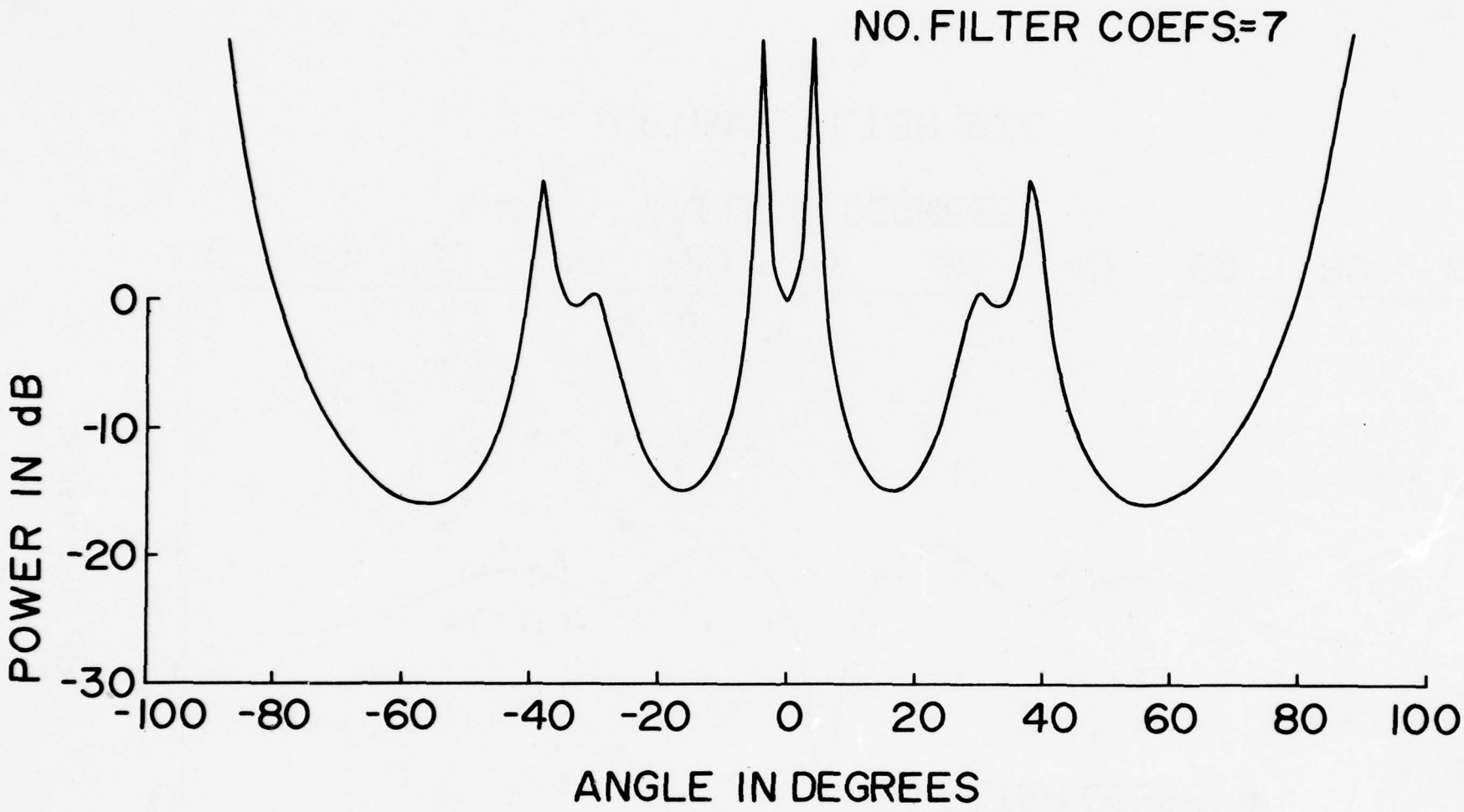
NO. FILTER COEFS.=7
POWER IN dB
0
-10
-20
-30
-100
-80
-60
-40
-20
0
20
40
60
80
100
ANGLE IN DEGREES

FIGURE 4f

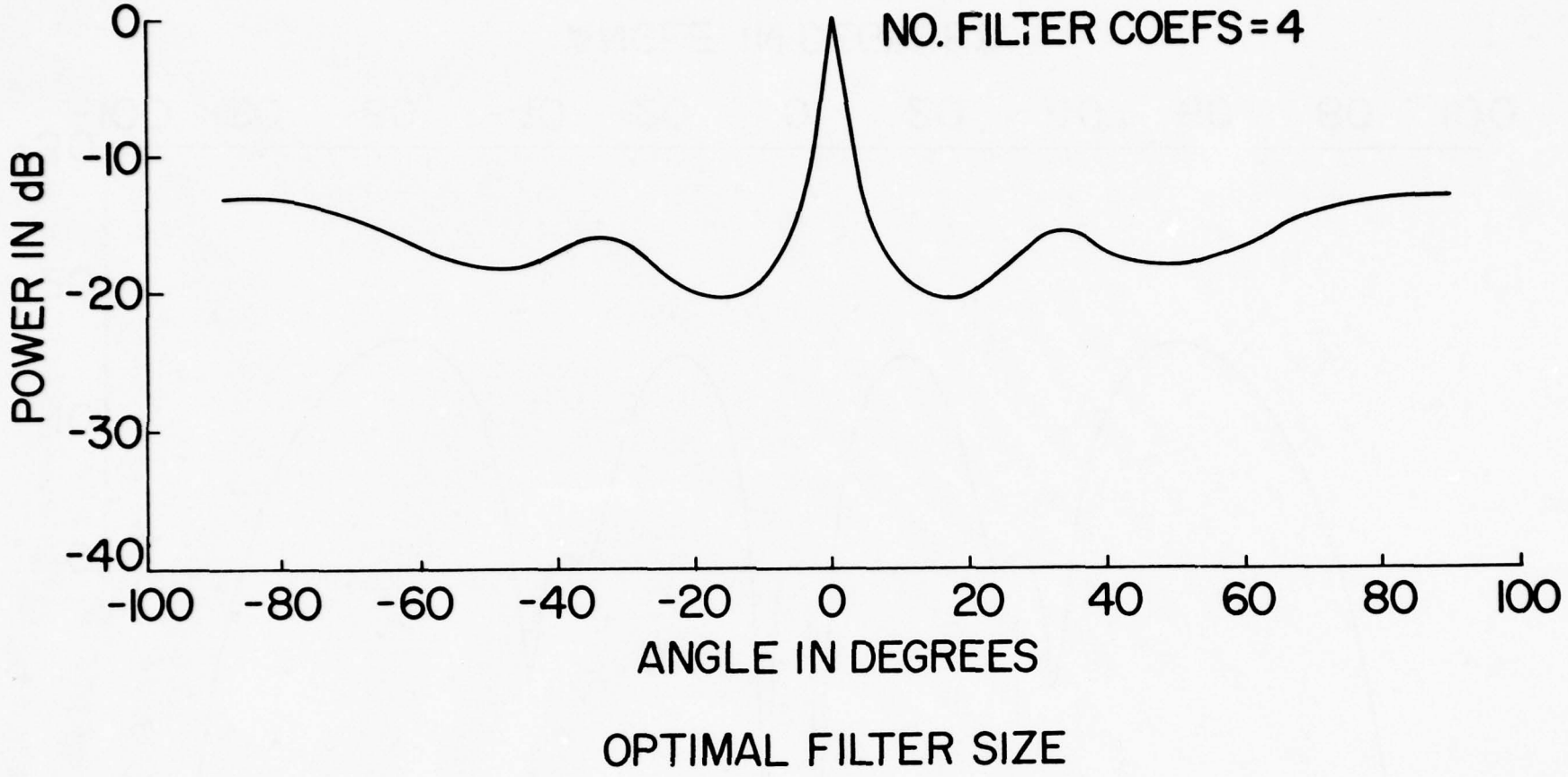
NO. FILTER COEFS = 4
POWER IN dB
0
-10
-20
-30
-40
-100
-80
-60
-40
-20
0
20
40
60
80
100
ANGLE IN DEGREES
OPTIMAL FILTER SIZE

FIGURE 4g

APPLICATION

SECTION III

Analysis

In order to demonstrate some of the MESA characteristics, antenna patterns are computed using the MESA-Burg technique hereafter referred to as just the MESA technique. In all MESA examples given, the King optimal filter is used so that all MESA antenna patterns are optimal in the sense that the automatically selected filter size allows each spectral component to have a maximum signal-to-noise (S/η) ratio.

The King optimal filter may also be used to select the optimal antenna pattern among the many patterns possible to compute in a given time period, but such a criteria is not used in obtaining the examples of this report. In order to minimize the number of spectra computed, antenna patterns exhibited are usually representative patterns, selected from a computed few and are neither the best nor the worst patterns possible with the use of MESA in a time varying noise field. In other examples as required, as many as ten patterns are computed and averaged to provide more representative examples.

Two Signals

Two signals each having (S/η) = 10.0 and separated two degrees are shown resolved by MESA in Fig. (5a) using a five element antenna having a total length of two wavelengths ($L = 2\lambda$). For comparison the antenna pattern shown in Fig. (5b) is computed for the same two signals and antenna using conventional phased array summation. As anticipated the conventional technique, which is computed for a 60 dB (S/η) level, does not resolve the two signals since the resolution of a two wavelength antenna is only about 22 degrees.

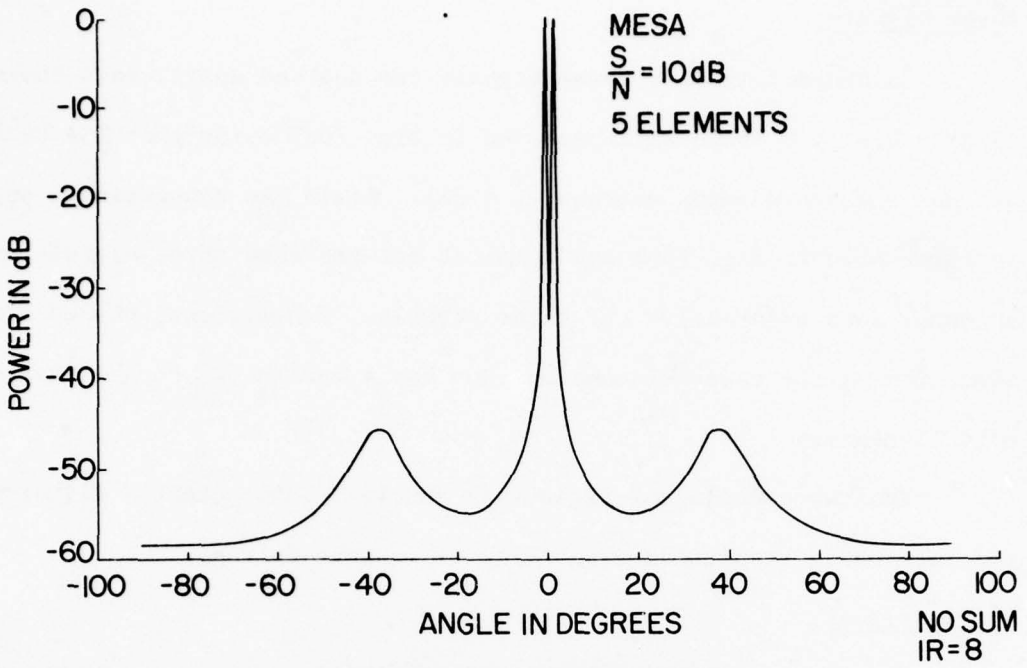

TWO CLOSELY SPACED SIGNALS

FIG. 5a

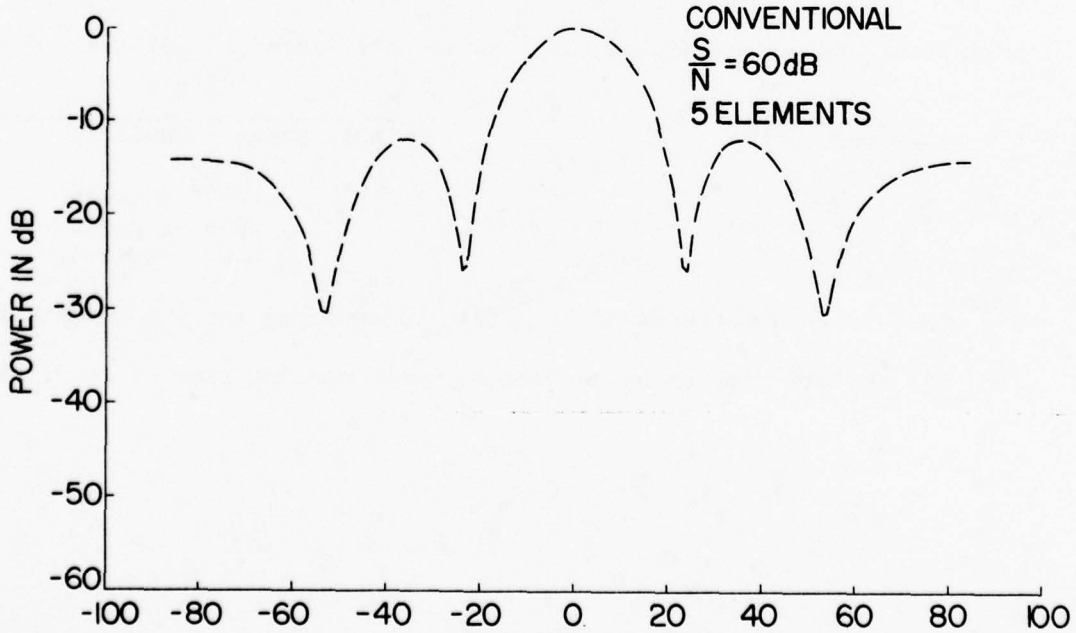

TWO CLOSELY SPACED FIGURES

FIG. 5b

Three Signals

In another example three signals two degrees apart, each having a $(S/\eta) = 0.5$, are shown well resolved in Fig. (6a) using the MESA technique and a seven element antenna ($L = 3\lambda$). Again the conventional antenna pattern shown in Fig. (6b) and computed for the same three signals and antenna, does not resolve the three signals. Conventional phased array summation of the seven element antenna has a resolution capability of only 15 degrees.

The two examples of Figs. (5a) and (6a) quite clearly illustrate the remarkable resolution capability of maximum entropy.

Single Signal

In order to obtain a better measure of the MESA resolution capability, a single signal at 0 degrees (broadside to the antenna) is magnified with an enlarged angular scale. Three such MESA antenna patterns shown superimposed in Fig. (7) serve to illustrate the MESA resolution as a function of the (S/η) ratio. The beamwidth of each peak is measured at the half power (3 dB) points on the peaks as an indication of typical MEAS resolution. The measured beamwidths and corresponding (S/η) ratios are listed as follows:

S/η (power ratio)	$(\Delta\theta)_{1/2}$ (Half power beamwidth)
10 dB	.0044 degrees
5 dB	.008 degrees
1 dB	.20 degrees

The three antenna patterns of Fig. (7) are computed for a 6 element antenna ($L = \frac{5}{2}\lambda$) and are plotted on an abcissa scale ranging from -1 to +1 degrees.

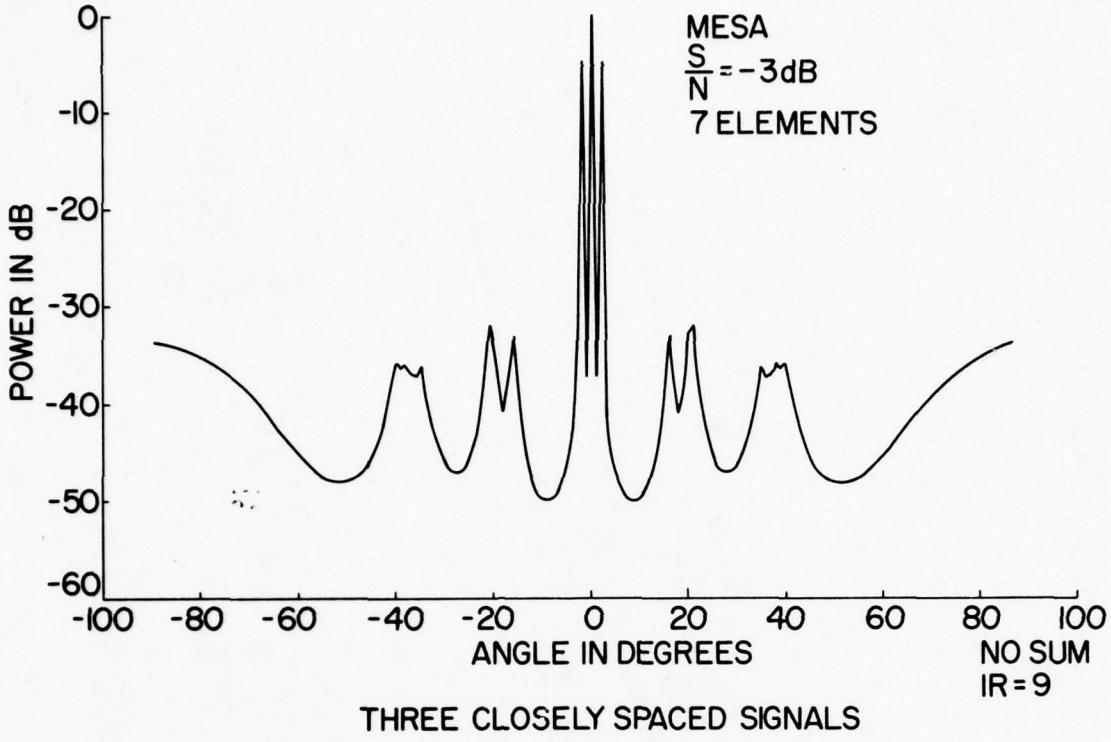
MESA
S/N = -3dB
7 ELEMENTS
POWER IN dB
0
-10
-20
-30
-40
-50
-60
-100 -80 -60 -40 -20 0 20 40 60 80 100
ANGLE IN DEGREES
NO SUM
IR = 9
THREE CLOSELY SPACED SIGNALS

FIG. 6a

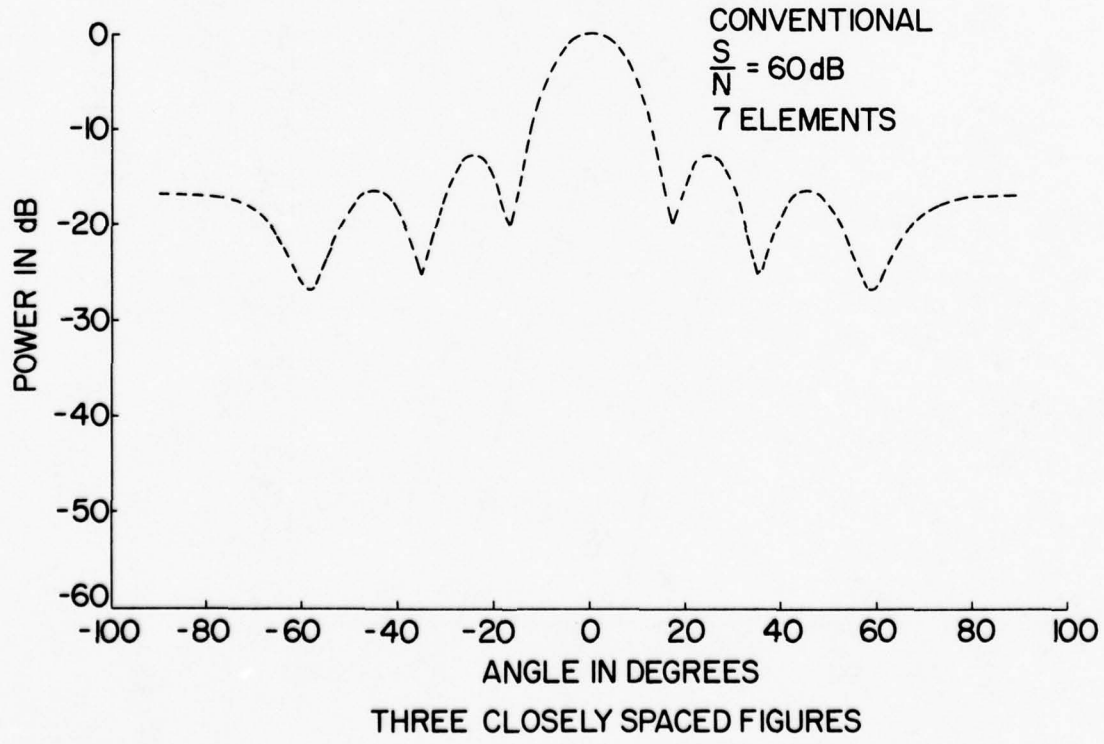
CONVENTIONAL
S/N = 60dB
7 ELEMENTS
POWER IN dB
0
-10
-20
-30
-40
-50
-60
-100 -80 -60 -40 -20 0 20 40 60 80 100
ANGLE IN DEGREES
THREE CLOSELY SPACED FIGURES

FIG. 6b

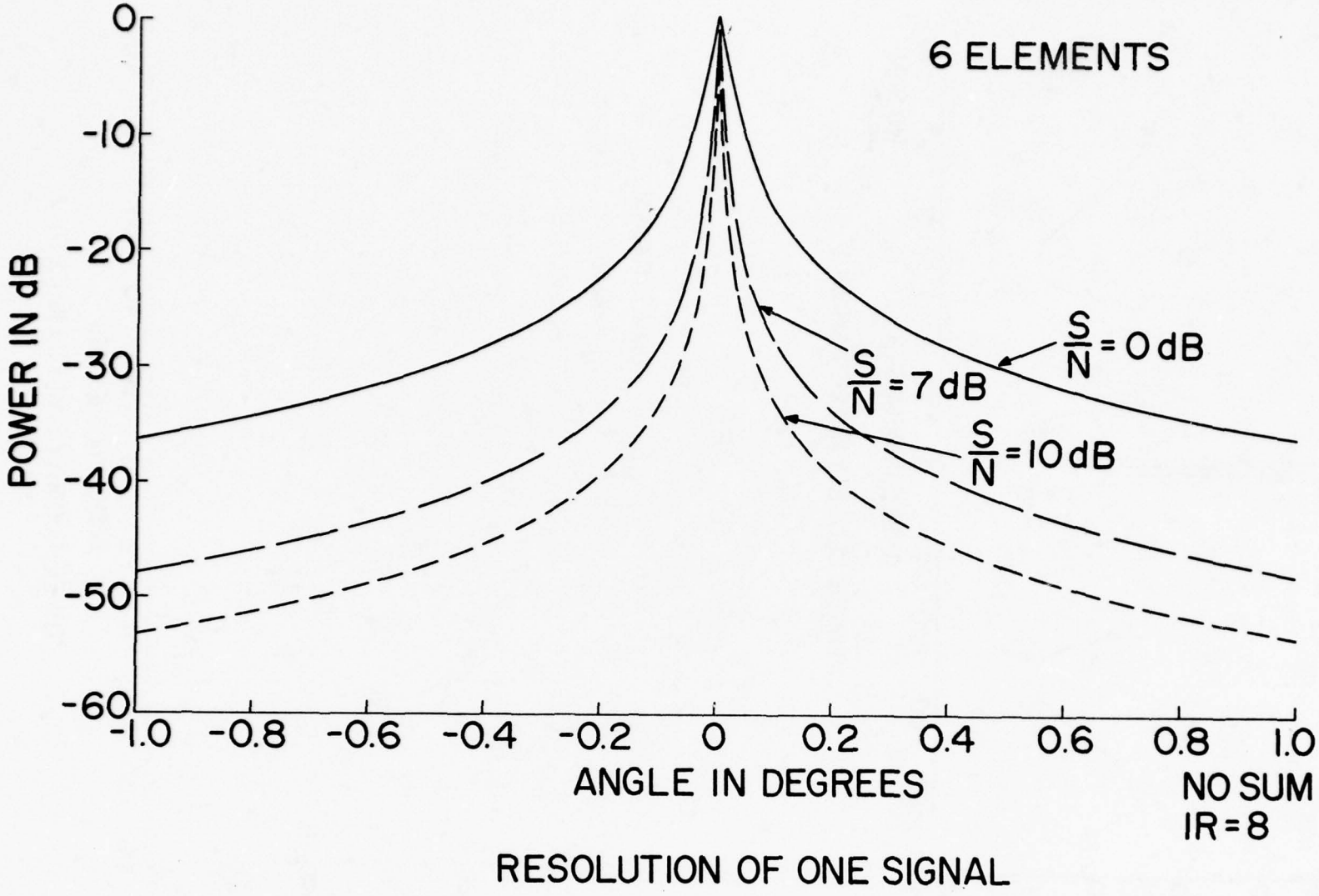

RESOLUTION OF ONE SIGNAL

FIG. 7

In order to demonstrate the functional relationship of beamwidth (or resolution) and (S/η) two curves computed for linear arrays having 6 and 24 elements as shown in Fig. (8). The curves are constructed through points representing half power beamwidths measured on magnified MESA antenna patterns computed for a range of (S/η) ratios. Also each curve is representative of only one particular set of noise data identified by the seed number (IR). The particular IR values indicated on the curves of Fig. (8) provided the best resolution out of 9 possible IR values tested ($1 \leq IR \leq 9$). However, the plotted resolution curves of Fig. (8) are neither the best nor the worst resolution possible for a given array size since only 9 cases of an infinite number of possible cases were examined.

MESA resolution is in fact highly sensitive to noise data samples such that other resolution curves, similar to those in Fig. (8) but for a different set of noise samples, may well be displaced toward higher or lower resolution values with resolution shifts of an order of magnitude. Consequently, the curves of Fig. (8) are merely representative curves without any statistical meaning. Of course such resolution curves should be constructed by averaging resolution points over some large number of computed MESA antenna patterns for which a σ is specified. However, a set of such meaningful and useful curves do require a considerable amount of computer time.

While the curves of Fig. (8) are not statistically meaningful, they do suggest that resolution values of the order of 0.1 to .0001 are obtainable with MESA with relatively short length antennas and reasonable (S/η) ratios.

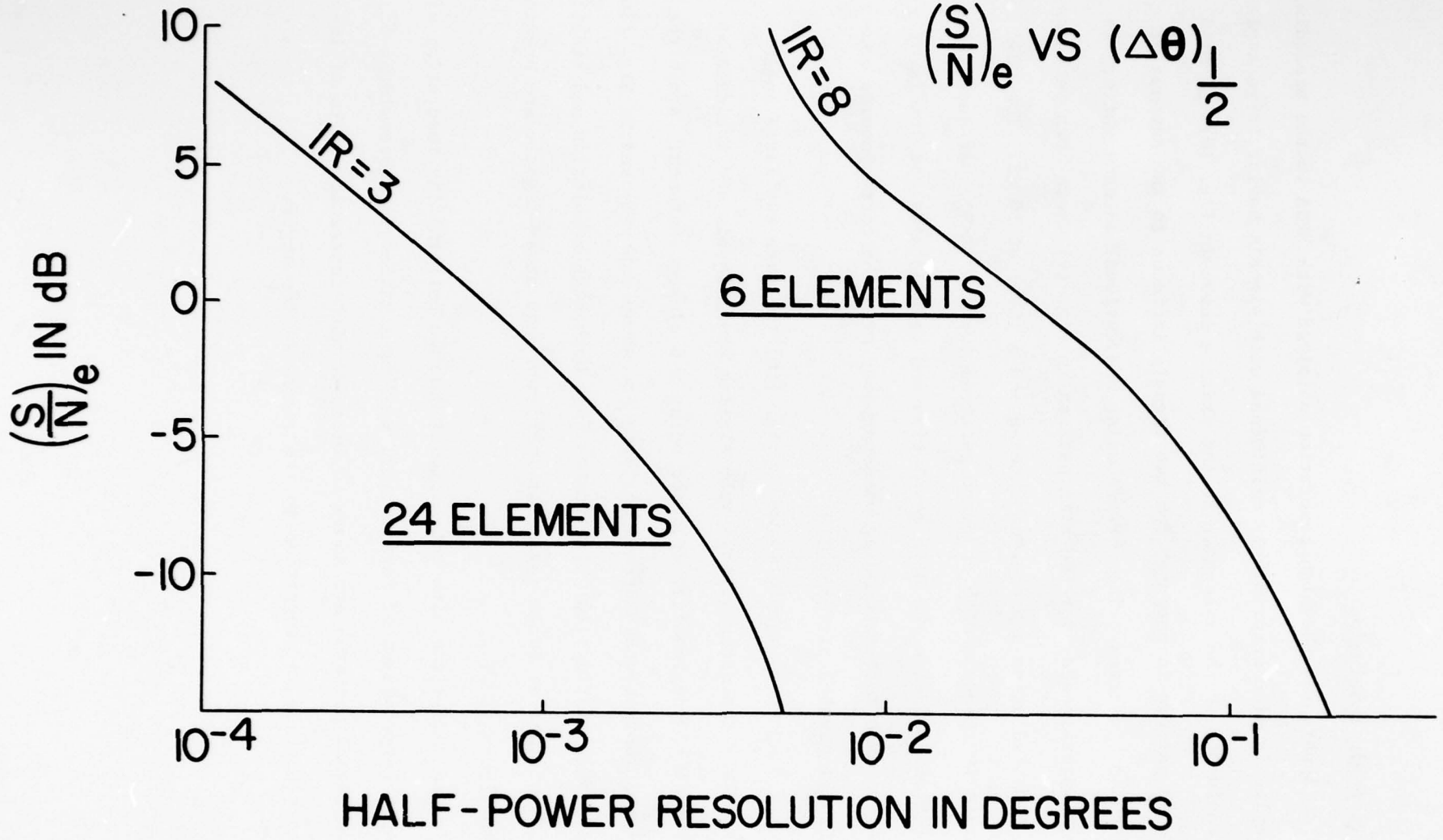
$\left(\frac{S}{N}\right)_e$ VS $(\Delta\theta)_{\frac{1}{2}}$
IR=8
IR=3
6 ELEMENTS
24 ELEMENTS
10
5
0
-5
-10
$\left(\frac{S}{N}\right)_e$ IN dB
10^{-4}
10^{-3}
10^{-2}
10^{-1}
HALF-POWER RESOLUTION IN DEGREES

FIG. 8

Large Angle Resolution

Apparently the high resolution obtained with MESA in the preceding examples is also surprisingly maintained with signals having large angles of incidence to the antenna. In the example shown in Fig. (9) the MESA antenna pattern is computed for two signals incident to the antenna at -85 and +85 degrees. The corresponding conventional antenna pattern is shown superimposed over the MESA pattern in Fig. (9) where both patterns are computed using a 6 element antenna and a (S/η) of 10 dB. The MESA pattern is the best of 9 computed patterns for $(1 \leq IR \leq 9)$. At such large angles of incidence the high resolution and reduced sidelobe levels of MESA are even more astounding when compared with the corresponding conventional antenna pattern.

In another example shown in Fig. (10) the same two large angle signals and two other signals with similar power levels and incident at angles of ± 20 degrees are detected using a 6 element antenna. Again the MESA and conventional antenna patterns are shown superimposed in Fig. (10). The example of Fig. (10) illustrates that both high resolution and stability are maintained at large angles of incidence when other signals are present at smaller angles.

In comparison with conventional antenna patterns the resolution of MESA at large angles of incidence is most remarkable since beamwidths of conventional patterns are known to increase with increasing angle of incidence roughly in proportion to the secant of the angle.

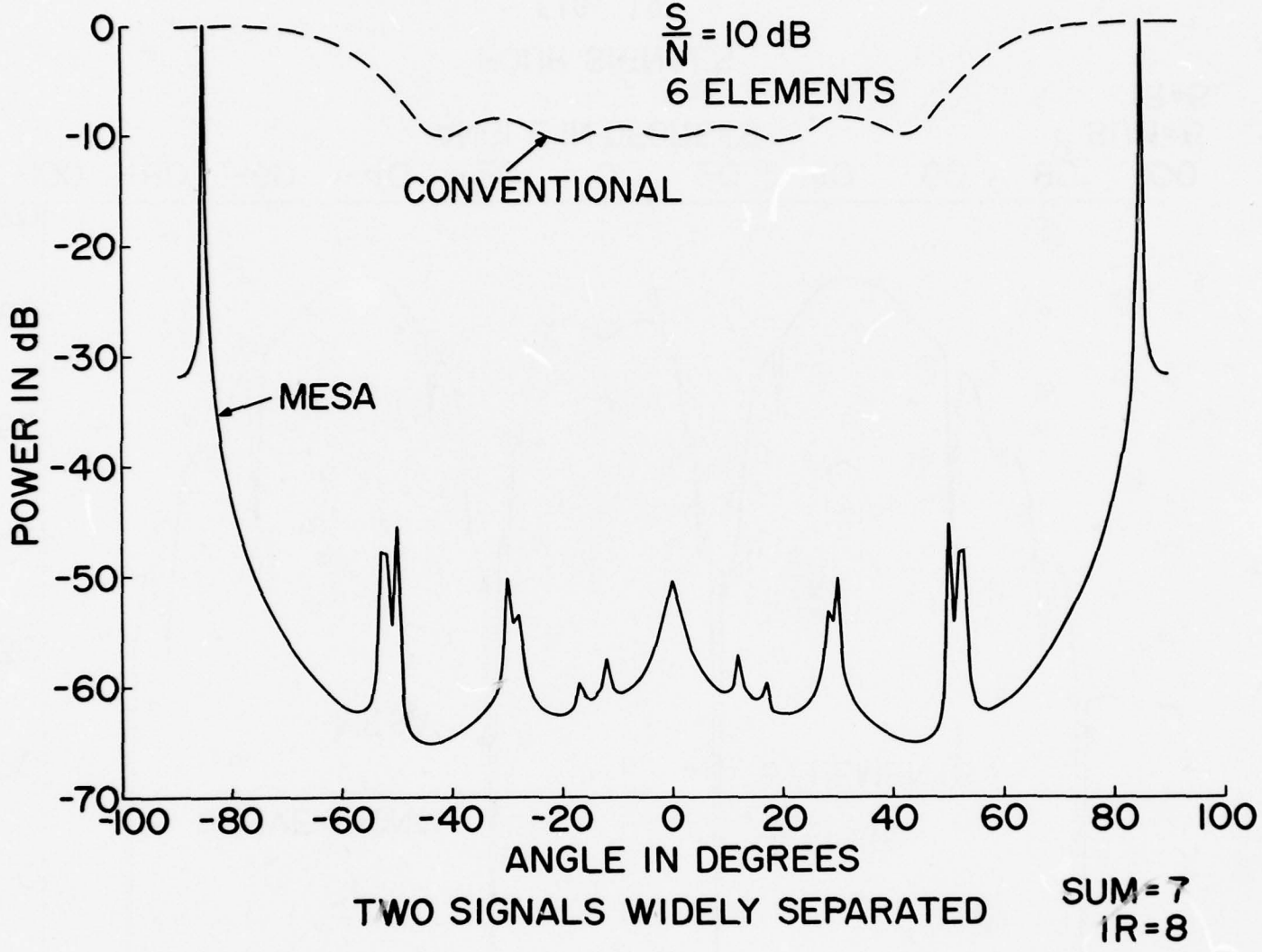
0
-10
-20
-30
-40
-50
-60
-70
POWER IN dB
S/N = 10 dB
6 ELEMENTS
CONVENTIONAL
MESA
-100
-80
-60
-40
-20
0
20
40
60
80
100
ANGLE IN DEGREES
TWO SIGNALS WIDELY SEPARATED
SUM = 7
IR = 8

FIG. 9

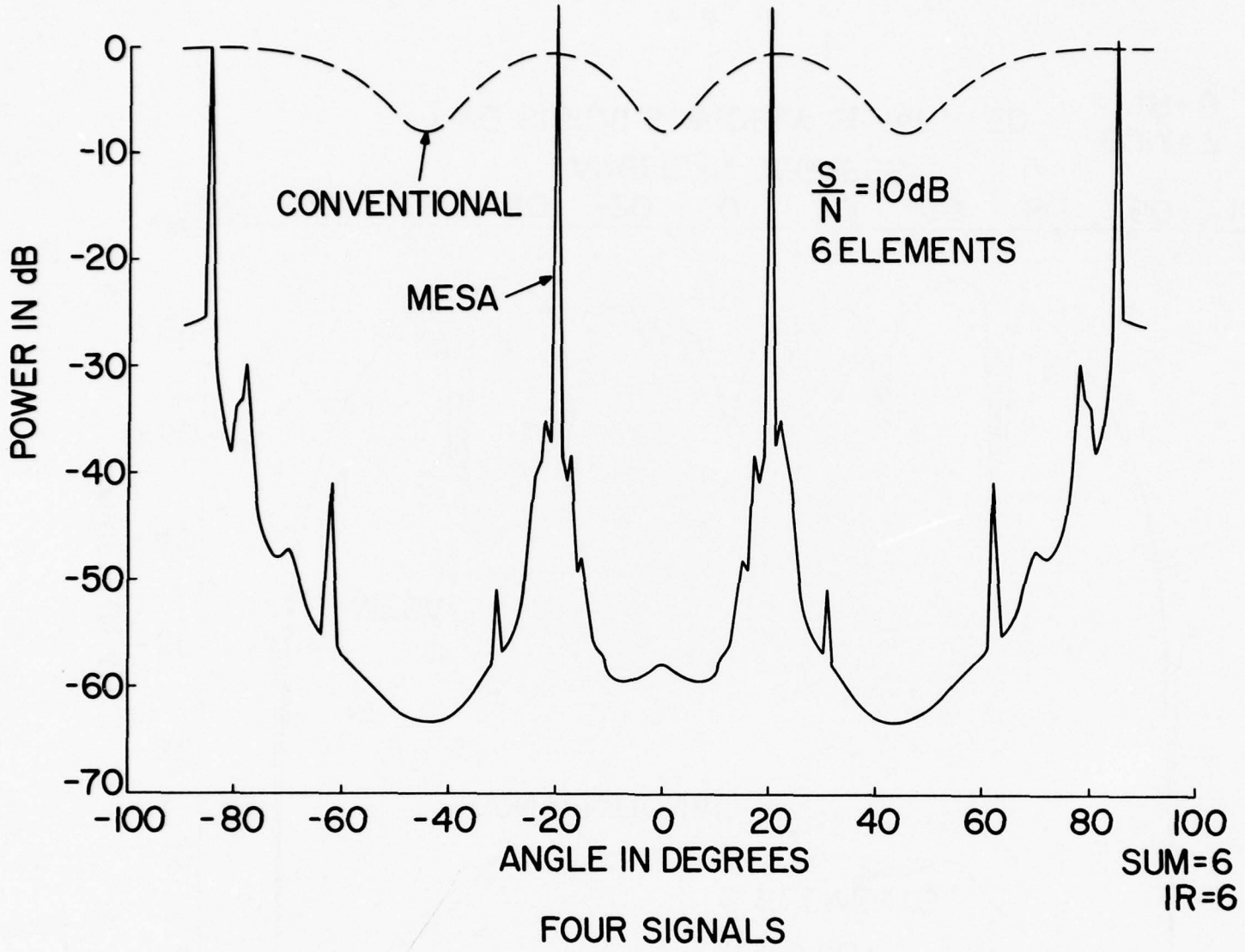

FOUR SIGNALS

FIG. 10

Multiple Signals

In order to establish the stability of MESA with an increasing number of signals incident to the antenna, antenna patterns are computed both with MESA and with conventional phased array summation for combinations of five and ten signals and for linear antenna arrays of 12 and 25 elements respectively. Both MESA and conventional antenna patterns are shown superimposed in Fig.(11)for five signals each having (S/η) = 10 dB and in Fig.(12)for ten signals each with (S/η) = 1.0 dB. As in all other MESA and conventional antenna patterns, phase of each antenna element is varied so as to "steer" or direct the antenna in the direction of each incident signal, and corresponding antenna patterns are computed in this manner for each signal,and all patterns are averaged together to obtain the one resulting pattern displayed. As a result the antenna patterns in Fig.(11)are actually five "steered" patterns averaged together.

All antenna patterns are displayed by computing points only for integer degree points so that each pattern consists of 181 computed points with points in between linearly extrapolated. Since the signals displayed in Figs.(11)and(12)all occur at integer angles the peak location or angular stability of MESA appears to be quite good in both figures. Almost every single signal peak is detected where anticipated with the apparent exception in Fig. (12) of signals located at -60 and 0 degrees. Apparently the -60 degrees signal is detected by MESA to be somewhere between -60 and -59 degrees, and the 0 degree peak which has noticeable assymetry in Fig. (12) is apparently detected by MESA to be

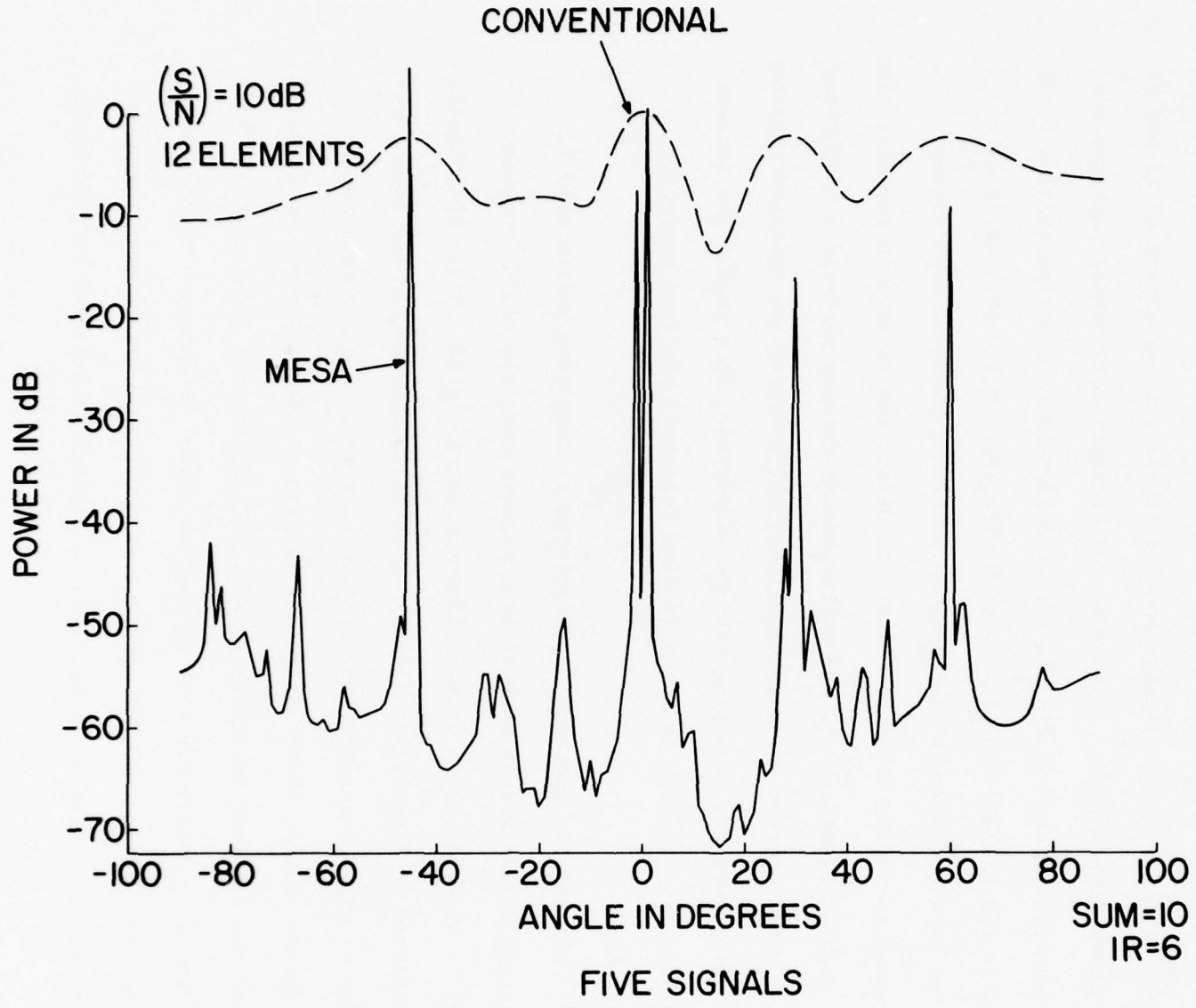

FIVE SIGNALS

FIG. 11

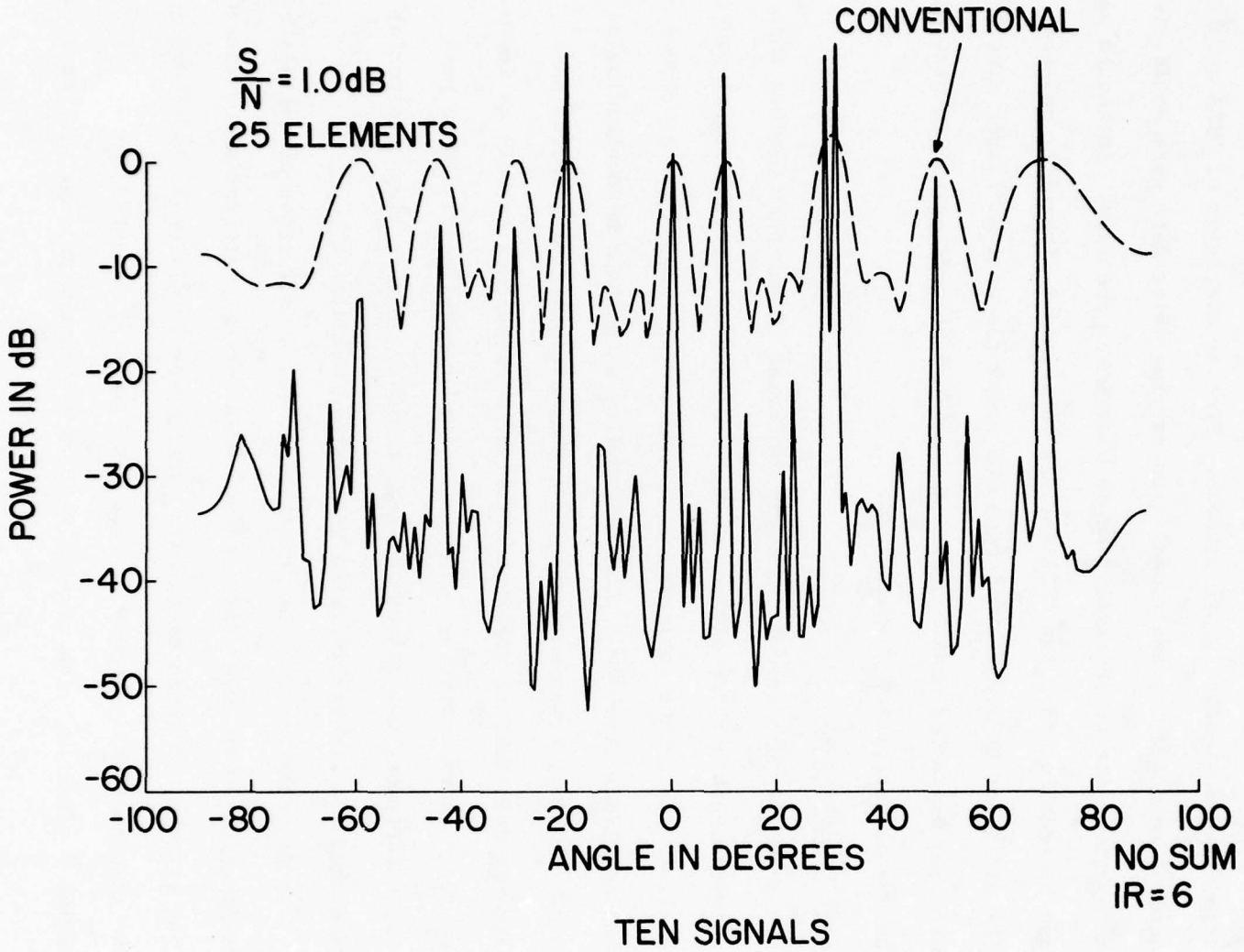
CONVENTIONAL
S/N = 1.0dB
25 ELEMENTS
0
-10
-20
-30
-40
-50
-60
POWER IN dB
-100 -80 -60 -40 -20 0 20 40 60 80 100
ANGLE IN DEGREES
NO SUM
IR = 6
TEN SIGNALS

FIG. 12

between 0 and +1 degrees. From such observations it is apparent that MESA suffers some even slight instability in signal peak location when large numbers of signals are present. Further averaging of MESA antenna patterns computed for additional time varying noise data sets would likely improve such slight instabilities in wavenumber accuracy. It should perhaps be recalled that the MESA antenna patterns of Figs. (11) and (12) are, like all other MESA patterns, computed using the optimal filter size so that each exhibited peak has optimal peak height and optimal resolution, and overall stability is maximized.

Mixed Power Levels

In all MESA antenna patterns exhibited it has been obvious that estimated peak heights are not well correlated with actual signal power levels. Peak height estimates with MESA are representative of either MESA non-linearities or a MESA instability or perhaps a combination of both. However, experience has shown that averaging of computed MESA patterns does tend to somewhat stabilize peak heights as well as improve the (S/η) characteristics. Instabilities or non-linearities in peak height estimates may affect the detectability of weak signals especially when they are accompanied with very strong signals.

In order to test the detectability of a collection of signals having substantial power level differences, MESA antenna patterns are computed for four signals, of which three have equal power levels where $(S/\eta) = 0$ dB. The resultant MESA pattern is shown in Fig. (13) computed for an antenna having 9 elements. The signals which are observed in Fig. (13) at their

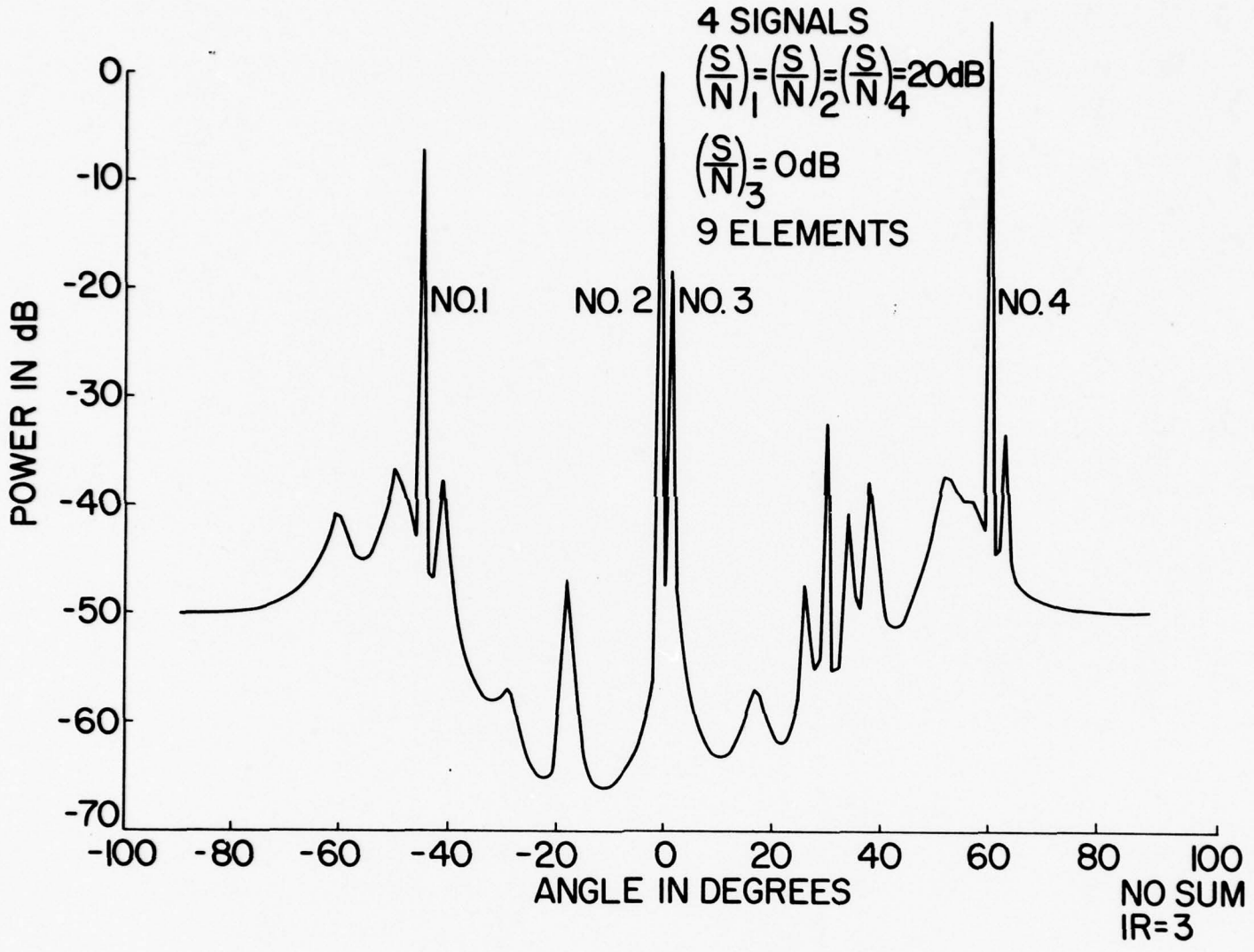

MIXED POWER LEVELS I

FIG. 13

correct angles of -45, -1, +1, +60 degrees, have the usual amplitude variations. The smallest of the four largest peaks, which is indeed the weaker signal, is 18 dB below the adjacent stronger signal. In an average over twenty such MESA antenna patterns (computed using 20 different noise data sets), the resultant antenna pattern shown in Fig. (14) is improved as expected. There is an overall gain in the output (S/η), and even some improvement (6 dB) in the relative peak height of the weaker signal occurring at +1 degrees.

In another example of signals with mixed power levels, a MESA antenna pattern shown in Fig. (15) is computed for an antenna with 12 elements and five signals, of which three have $(S/\eta) = 20$ dB and two have $(S/N) = 0$ dB. However, in the resulting MESA pattern only three of the signals located at -45, +1 and 60 degrees are obviously detectable in Fig. (15). Of the two weaker signals located at -1 and 30 degrees, only the one at -1 degrees could possibly be considered as a signal candidate. In fact the signal incident at +30 degrees is well into the background noise.

In an average of twenty MESA patterns computed for the same five signals and the same 12 element antenna, it is observed in Fig. (16) that there is again considerable overall improvement in (S/η) levels, and also there is considerable improvement in the relative peak height of the weaker signal located at +30 degrees. On the other hand there is no apparent improvement in the detectability of the weaker signal located at -1 degrees.

The examples of Figs. (13-16) are an indication that weak signals may or may not be detectable with MESA when they occur in the company of considerably stronger (20 dB) signals. But it is also evident that pattern

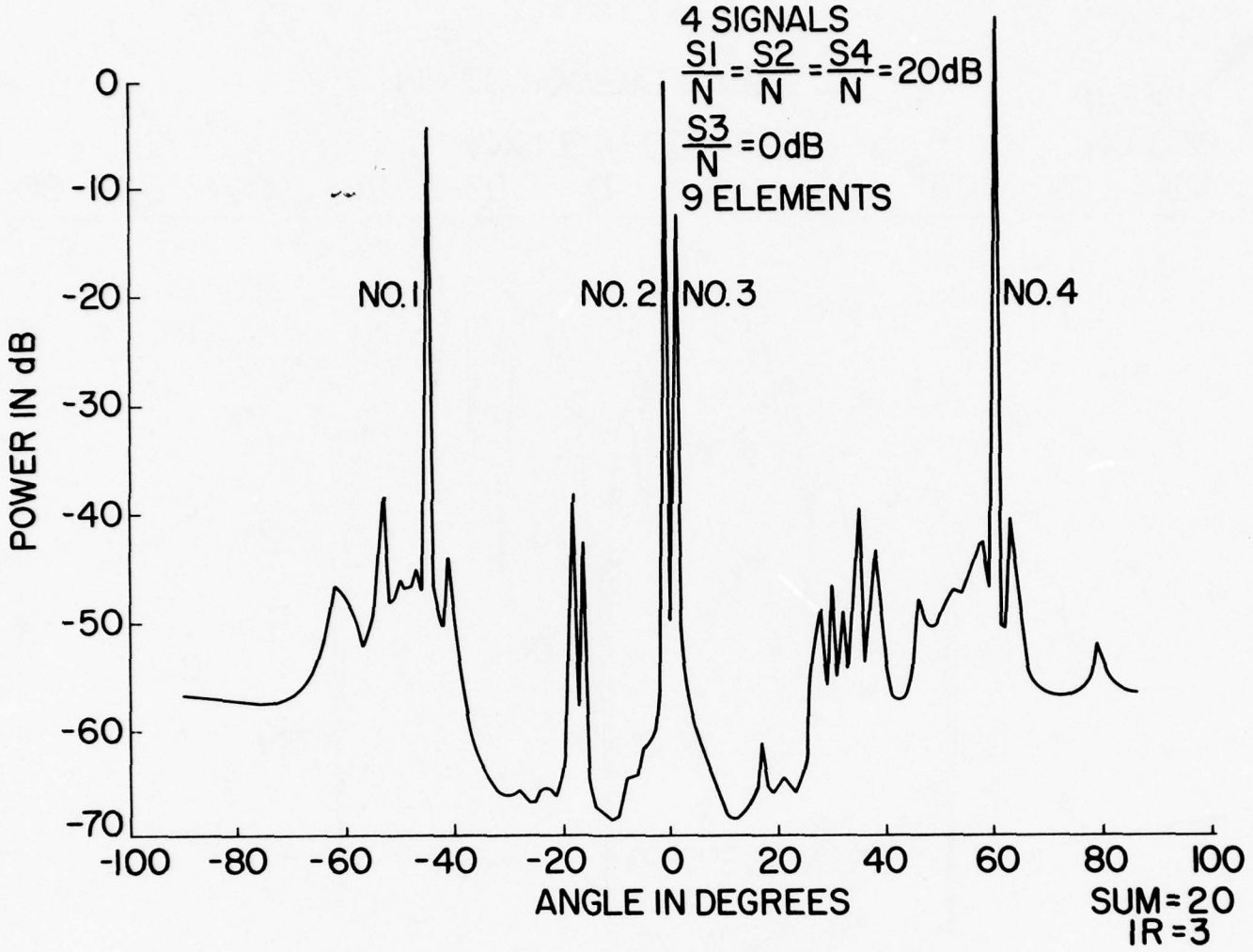

MIXED POWER LEVELS I (SUM = 20)

FIG. 14

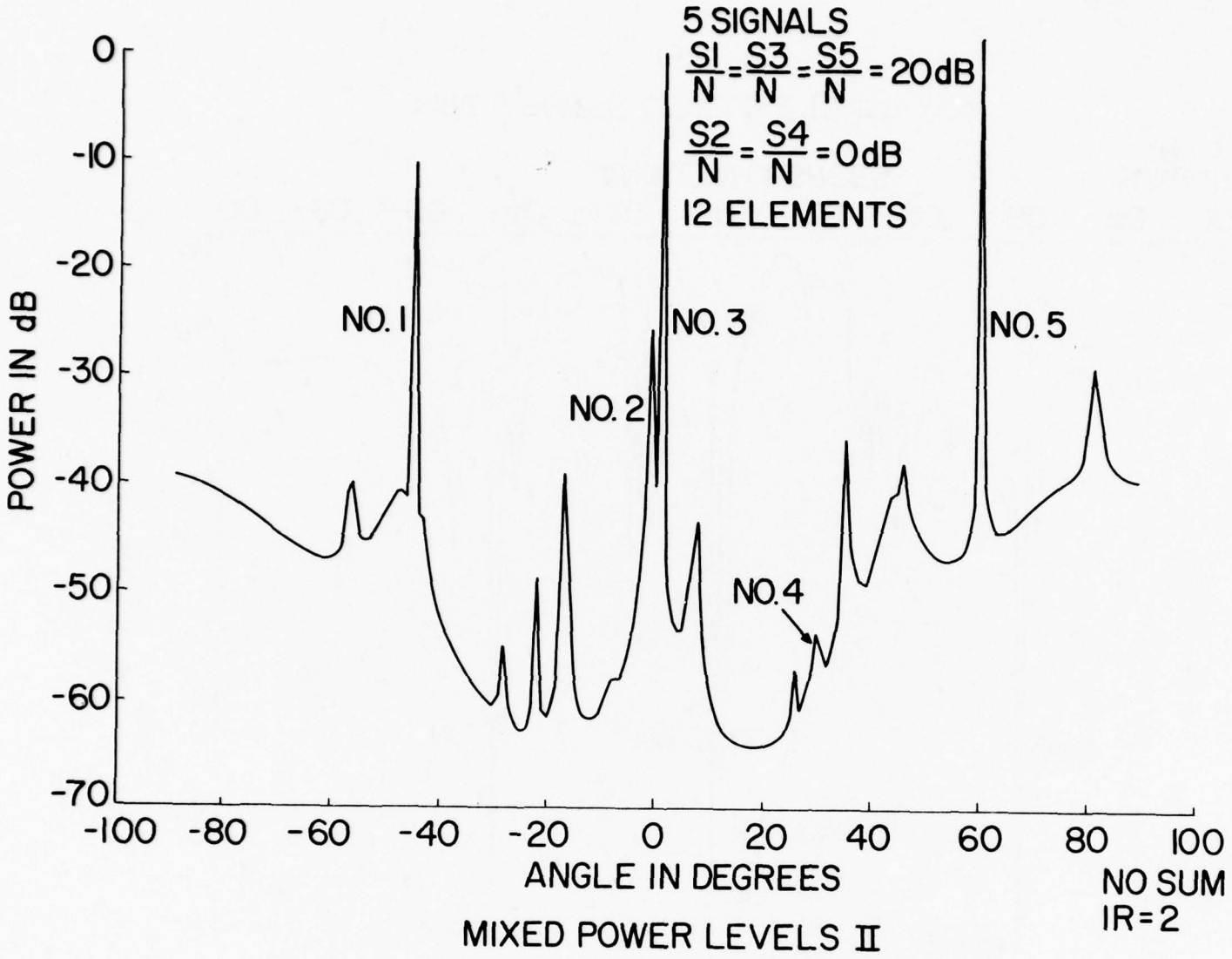
5 SIGNALS
S1/N = S3/N = S5/N = 20dB
S2/N = S4/N = 0dB
12 ELEMENTS
NO. 1
NO. 2
NO. 3
NO. 4
NO. 5
POWER IN dB
0
-10
-20
-30
-40
-50
-60
-70
-100
-80
-60
-40
-20
0
20
40
60
80
100
ANGLE IN DEGREES
NO SUM
IR=2
MIXED POWER LEVELS II

FIG. 15

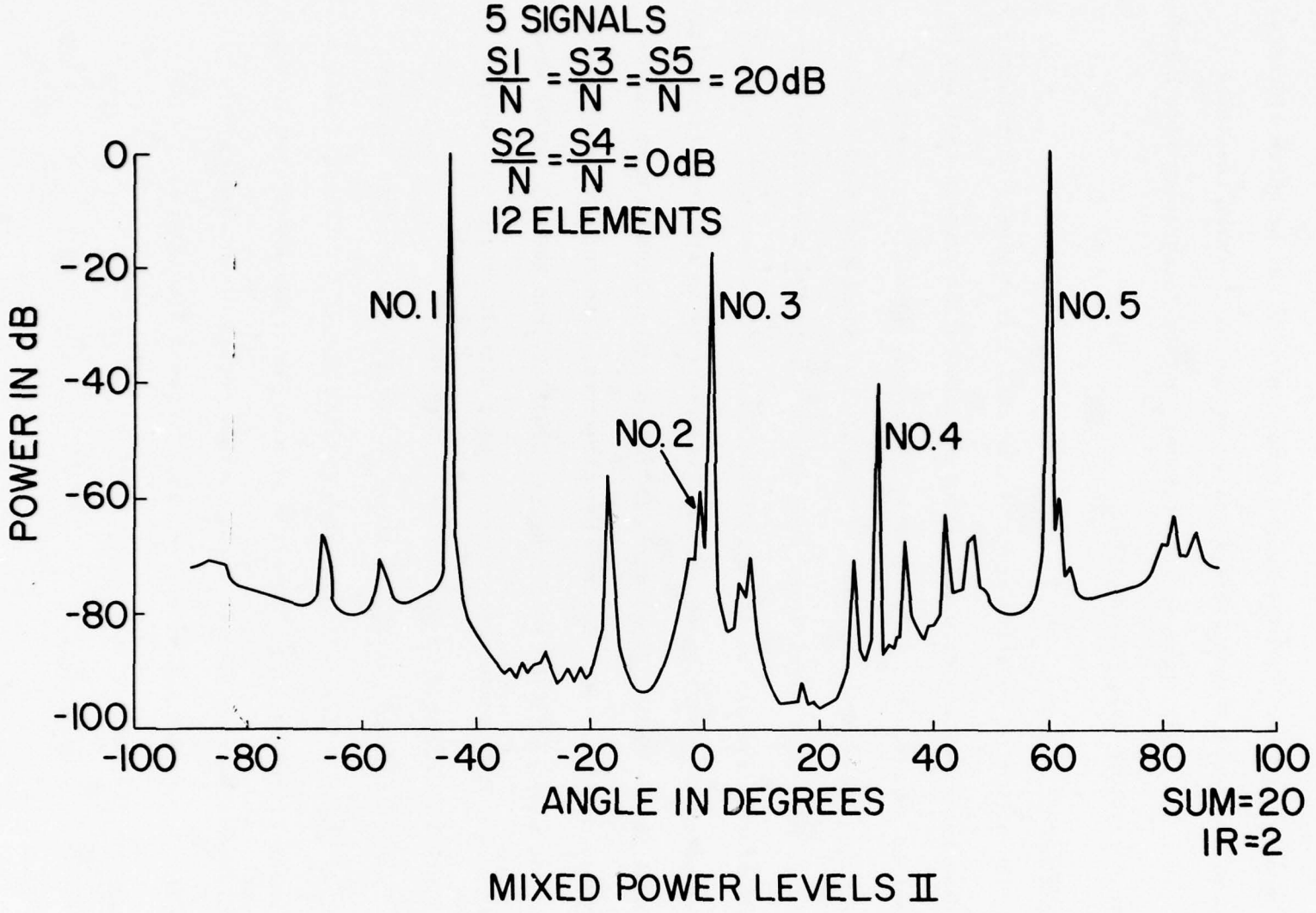
5 SIGNALS
S1/N = S3/N = S5/N = 20dB
S2/N = S4/N = 0dB
12 ELEMENTS
NO. 1
NO. 2
NO. 3
NO. 4
NO. 5
POWER IN dB
0
-20
-40
-60
-80
-100
-100 -80 -60 -40 -20 0 20 40 60 80 100
ANGLE IN DEGREES
SUM=20
IR=2
MIXED POWER LEVELS II

FIG. 16

averaging may enhance the relative peak level and hence the detectability of such weak signals. Perhaps longer term averaging may be quite effective with MESA even though such averaging also serves to increase the false alarm rate. No doubt there is some optimal pattern integration time based upon an acceptable false alarm rate.

Relative Signal Phase

The effect of relative signal phase shifts is a significant factor affecting the detection of a collection of interfering signals that may be incident to an antenna. Unfortunately it is only possible to examine a few relative phase shift examples. However, two phase shifts of π and $\pi/4$ are perhaps more significant than others due to the possibility that two interfering signals having a relative phase difference of π may totally or even partially cancel each other. Also there is an apparent instability with MESA in the detection of phase shifted signals which is most severe at a phase shift of $\pi/4$. Several investigators, Chen and Stegen (1974), Ulrych and Clayton (1976), and Fougere, Zawalick, and Radoski (1976) have all noted the MESA phase shift instability. Signals having both phase shifts are investigated in the following examples.

A MESA antenna pattern is shown in Fig. (17) where five signals having no phase shifts (all have zero initial phase) are detected with a 12 element linear antenna. The five signals, each having $(S/\eta) = 10$ dB, are all detected with MESA at their correct angles of incidence, -45, -1, +1, +30, +60 degrees. However, as usual the peak levels are not equal even though all signals have equal powers.

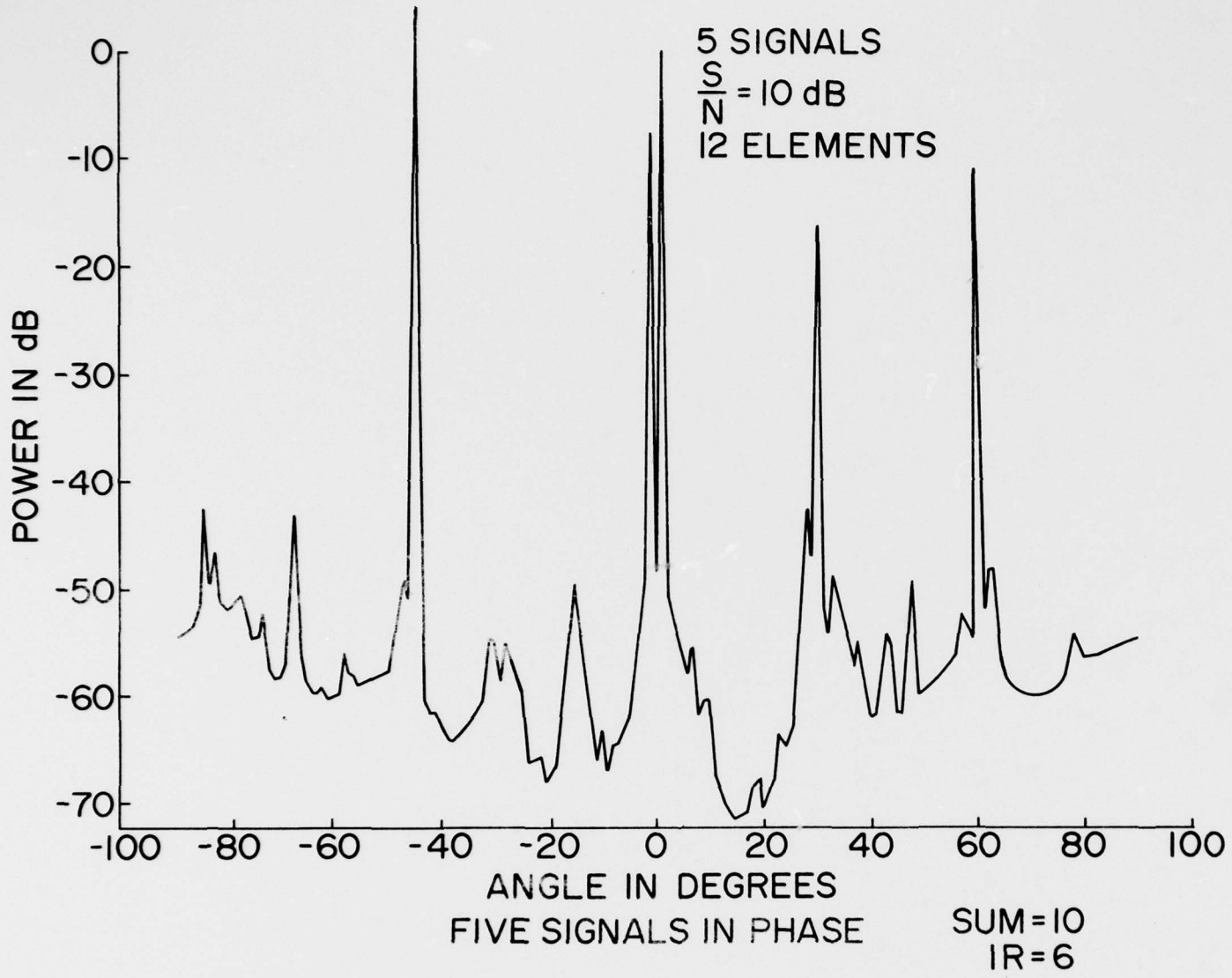
5 SIGNALS
S/N = 10 dB
12 ELEMENTS
POWER IN dB
0
-10
-20
-30
-40
-50
-60
-70
-100
-80
-60
-40
-20
0
20
40
60
80
100
ANGLE IN DEGREES
FIVE SIGNALS IN PHASE
SUM = 10
IR = 6

FIG. 17

For the same set of signals one signal, at +1 degrees is given a phase shift of π relative to all other signals and the resultant MESA antenna pattern is shown in Fig. (18), where it is noticed that the two adjacent signals located at -1 and +1 degrees have greatly reduced peak levels. The other three signals are apparently not affected by the phase shifted signal It appears that the two closely adjacent signals having opposite polarity have effectively canceled one another. Even though the MESA pattern in Fig. (18) represents an average of ten patterns, the effect of pattern averaging has not overcome the phase shift interference between the two adjacent signals. Of course the same effective signal cancellation is also noticed in conventional antenna patterns.

In another example of the identical collection of signals, where the one signal at +1 degrees has a relative phase shift of π, but with an entirely different set of noise data (IR = 7), the computed and averaged MESA antenna pattern is shown in Fig. (19), where only the signal at +1 degrees with the phase of π is reduced beyond recognition. The closely adjacent signal, and the other widely separated signals all having zero phase, are all readily detectable. While one example, which includes some pattern averaging, indicates that two nearby signals having a relative phase of π tend to cancel one another, another example has indicated that one of the signals may be detected. Since other examples not shown have indicated that one or both of the closely spaced signals is often detectable, it is concluded that a relative phase shift of π is a problem with MESA in that such relative phase shifts may reduce the detectable of one or more signals. However, it is also concluded that long term pattern averaging does serve to restore some of the loss in peak levels.

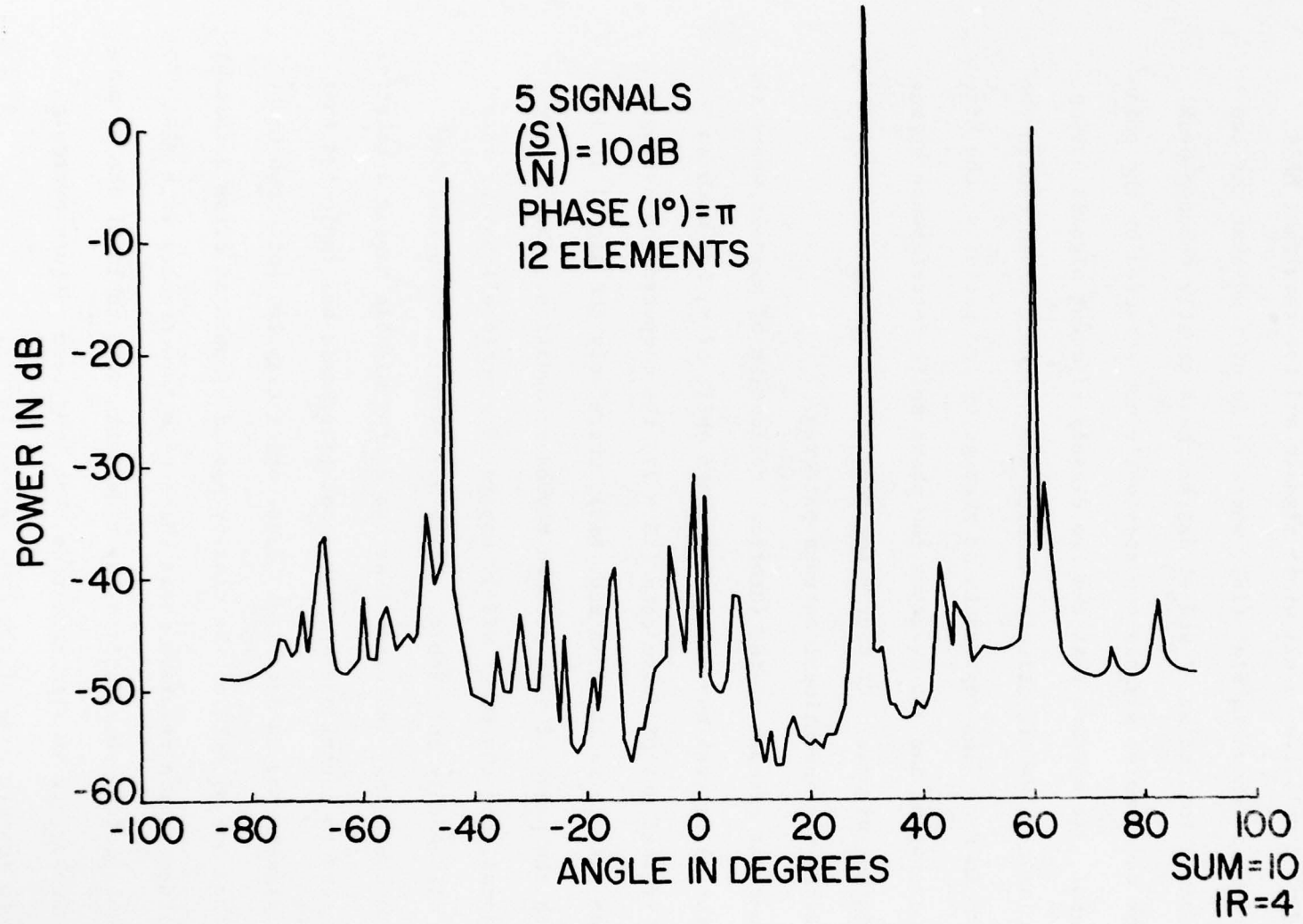

EFFECT OF PHASE SHIFT I

FIG. 18

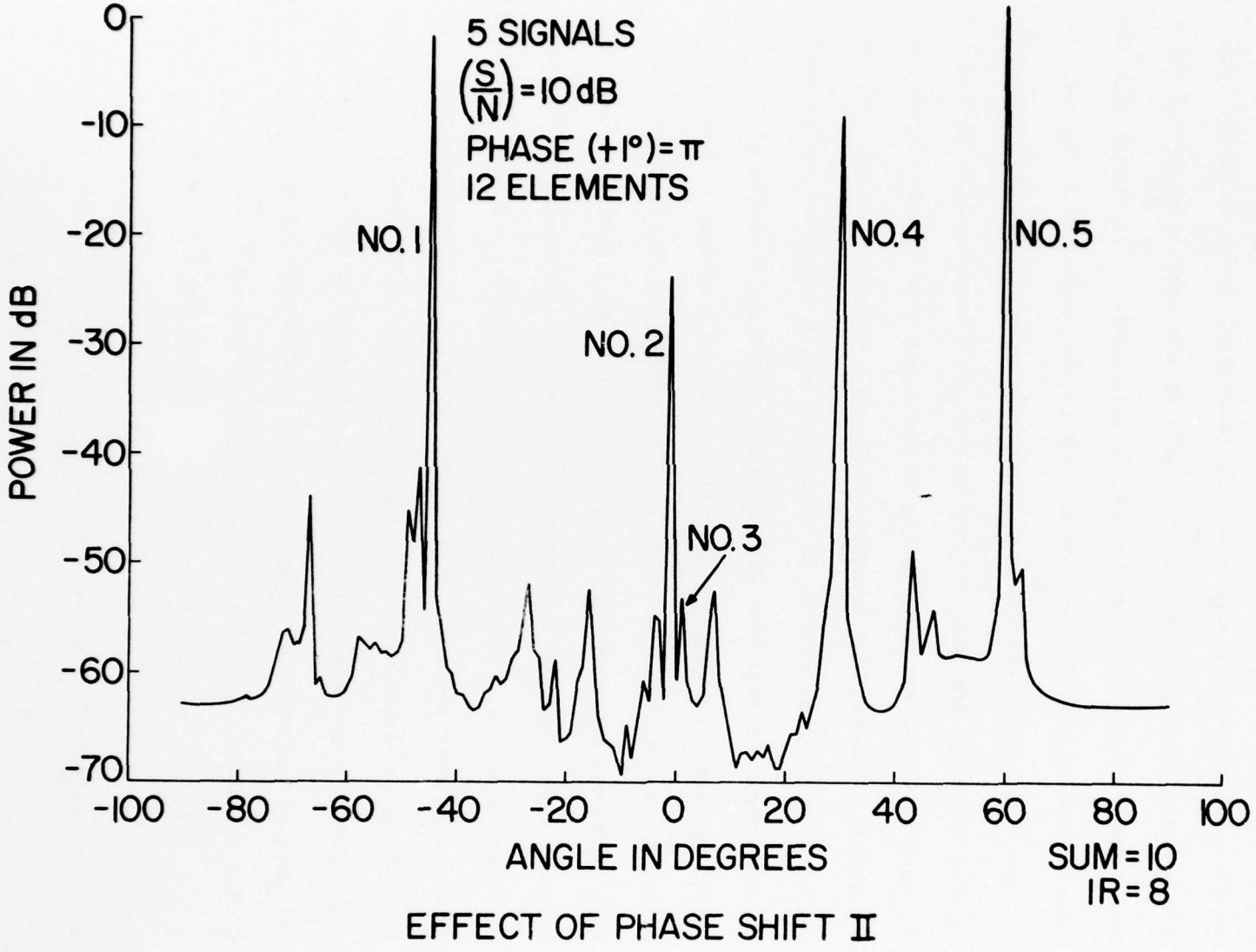

EFFECT OF PHASE SHIFT II

FIG. 19

MESA is tested further where the signal located at +30 degrees is given a phase shift of $\pi/4$ relative to all other signals having zero initial phase. The resultant MESA antenna is shown in Fig. (20) computed for the same antenna (12 elements) and same (S/η) ratio of 10 dB. All five signals which are located precisely at the correct angles of incidence appear in Fig. (20) to be readily detectable. The signal with the phase of $\pi/4$ is quite evident at the +30 degree angle and is apparently not the cause of any instability. As in the two previous MESA patterns of Figs. (18-19), the MESA pattern in Fig. (20) represents an average of ten such patterns, since averaging is desirable when instabilities are suspected. However, the instability due to a signal phase of $\pi/4$, which has been reported by others, is apparently not a source of any instability in the example of Fig. (20) and, in fact, cannot be a source of peak splitting since the King optimal filter size is utilized. Since peak splitting appears to be a factor only at the larger filter sizes, the King technique automatically selects the filter size having the best possible (S/η) ratio at the correct peak location determined by a previous root determination at some stable lower filter order; and since split peaks have a very poor value of (S/η) at the correct peak location, such instabilities are avoided with the optimal filter. As a further check, other (S/η) ratios have been utilized in an examination of the exact same signal set used in the example of Fig. (20) and as expected the split peak instability apparently just does not occur for the reason given.

While the two relative phase shifts examined are apparently not a source of instability in accurately locating signals (determining signal angles), phase shifts may be responsible for an instability in estimated

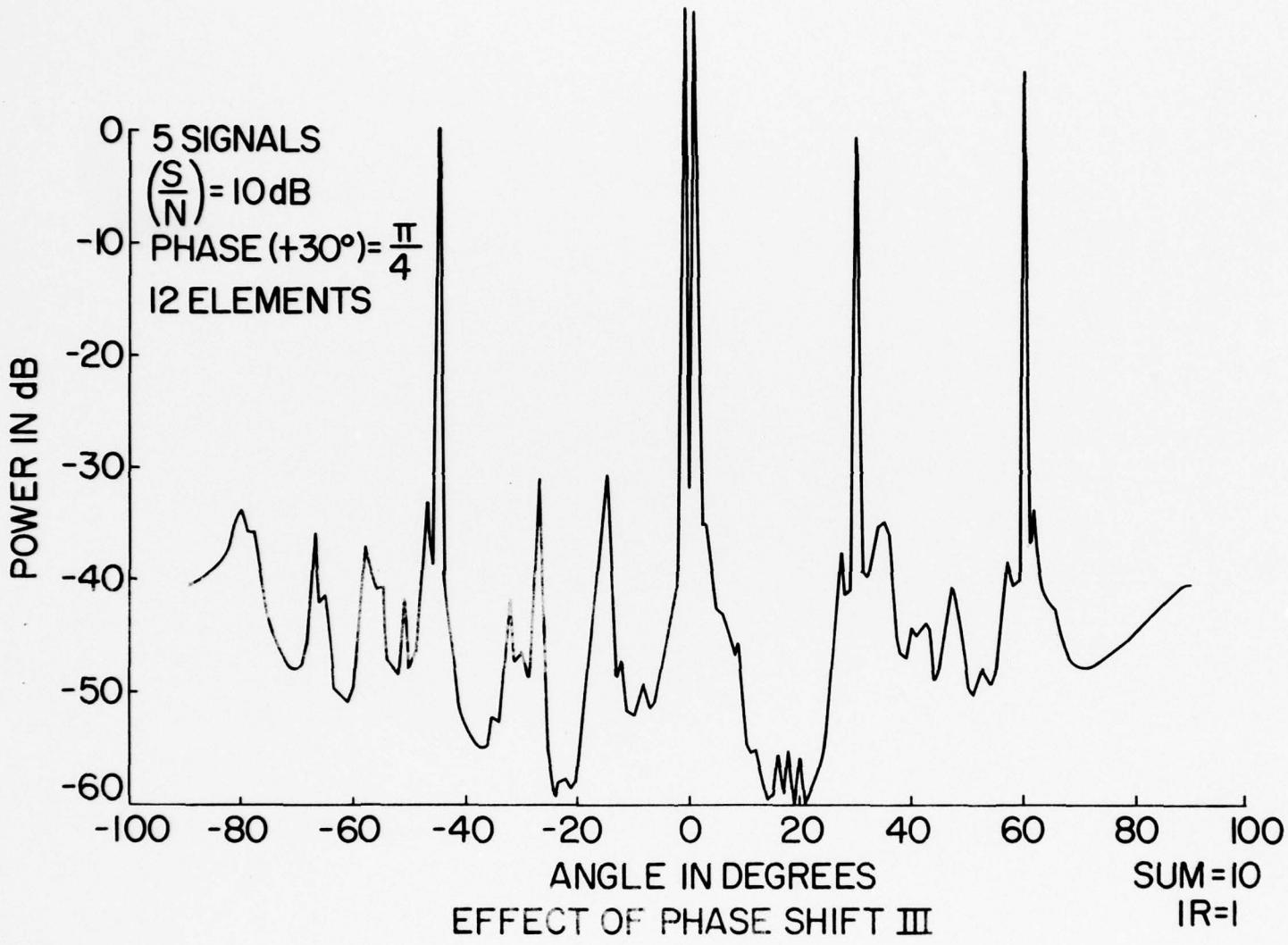
0
-10
-20
-30
-40
-50
-60
POWER IN dB
5 SIGNALS
(S/N) = 10dB
PHASE (+30°) = π/4
12 ELEMENTS
-100
-80
-60
-40
-20
0
20
40
60
80
100
ANGLE IN DEGREES
SUM = 10
IR = 1
EFFECT OF PHASE SHIFT III

FIG. 20

peak levels. In other words signals having initial phases other than zero may be a factor of contention in the detection of signals analyzed with MESA. However, pattern averaging is apparently helpful in alleviating any loss in signal detectability.

Summary

Desirable antenna pattern characteristics include high resolution, accurate angular prediction, peak detection at low (S/η) levels, and stability under noisy conditions and multiple target environments. In this necessarily encompassing and cursory investigation, antenna patterns computed using MESA have exhibited these desirable properties to a relatively high degree of measure.

Resolution with MESA is exceptional even under noisy conditions and in multiple and mixed target environments. High resolution is maintained even at very large angles of incidence. Estimates of signal angle appear to be quite accurate even under difficult signal conditions, and peak detection with MESA is obviously better than that provided by the Fourier transform. However, it is perhaps most significant that MESA exhibits good stability properties with use of the optimal filter size.

Non-zero signal phase does apparently affect signal levels and consequently signal detectability in an adverse manner, although averaging over many antenna patterns does help to restore the affected signal levels. The problem of peak splitting is apparently avoided although not corrected with use of an optimal filter order.

It can only be concluded that MESA is a most promising signal processing technique as it appears to provide significant improvements over conventional techniques for processing phased array antenna data.

While the results of this investigation demonstrate that MESA may be used to obtain very desirable antenna patterns, MESA characteristics are not defined in a precise manner. Hopefully, further investigations will establish MESA characteristics in a more definitive manner.

When new techniques provide significant improvements in certain characteristics, it is always suspected that other characteristics are degraded. Of course, usually such suspicions are well founded. However, the Maximum Entropy Spectral Analysis technique developed by Burg appears to have withstood most of the usual criticisms.

APPENDICES

SECTION IV

APPENDIX A

Prediction Filter

Consider a signal x(t) with a waveform only over the time interval (o,T). The waveform may be predicted (or estimated) for points outside the window (o,T) using the prediction filter in a convolution with the known signal x(t) as follows:

$$\hat{x}(t) = \int_o^T a(\tau)\, x\,(t - \tau)\, d\tau \qquad \text{(A1)}$$

where $\hat{x}(t)$ is the predicted signal and $a(\tau)$ is the impulse response of the prediction filter.

If the signal has been adequately sampled within the time interval (o,T) such that

$$\Delta t \leq 1/2f; \quad \frac{(M-1)}{T} \leq 2f$$

for a sampling interval Δt, M data samples, and signal frequency f, then the discrete convolution may be employed as follows:

$$\hat{x}_k = \sum_{n=1}^{N} a_n\, x_{k-n}, \quad N < M \qquad \text{(A2)}$$

where the summation is taken over N filter coefficients, N being less than the number of data samples.

Prediction Error Filter

An error ε_k may be defined for the known set of data samples as follows:

$$\begin{aligned} \varepsilon_k &= x_k - \hat{x}_k \\ &= x_k - \sum_{n=1}^{N} a_n x_{k-n} \qquad \text{(A3)} \\ &= \sum_{n=o}^{N} \gamma_n x_{k-n} \quad \text{for } \gamma_o = 1,\ n = 0 \\ &\qquad\qquad \gamma_n = a_n,\ n > 0 \end{aligned}$$

where γ_n is the n^{th} prediction error filter coefficient.

The squared error is expressed as follows:

$$\varepsilon_k^2 = \sum_{m=o}^{N} \sum_{n=o}^{N} \gamma_n \gamma_m \, x_{k-n} \, x_{k-m} \tag{A4}$$

since $\gamma_o = 1$ there are N remaining unknown prediction error coefficients. These N coefficients may be determined by minimizing the total mean squared error E_N which is defined as follows:

$$E_N = \frac{1}{2N+1} \sum_{k=-N}^{N} \varepsilon_k^2 \tag{A5}$$

The summation is taken over all errors possible to compute in a forward prediction within the data window defined by 2N+1 data samples. The incorporation of Eq. (A4) into (A5) results in the following equation:

$$E_N = \frac{1}{2N+1} \sum_{k=-N}^{N} \sum_{m=o}^{N} \sum_{n=o}^{N} \gamma_n \gamma_m \, x_{k-n} x_{k-m}$$

$$= \sum_{m=o}^{N} \sum_{n=o}^{N} \gamma_n \gamma_m \, \frac{1}{2N+1} \sum_{k=-N}^{N} x_{k-n} x_{k-m} \tag{A6}$$

$$E_N = \sum_{m=o}^{N} \sum_{n=o}^{N} r_{m-n} \, \gamma_n \gamma_m$$

where r_{m-n} represents the data set autocorrelation coefficients.

The prediction error coefficients are defined with minimization of the total prediction error as follows:

$$\frac{\partial E_N}{\partial \gamma_k} = 2 \sum_{n=o}^{N} \gamma_n \, r_{k-n} = 0 \tag{A7}$$

$$\text{for } k = 1, 2, 3, \ldots N$$

The resulting N equations with N unknowns are as follows:

$$k = 1,\ \gamma_o r_1 + \gamma_1 r_o + \gamma_2 r_1 + \ldots + \gamma_N r_{N-1} = 0$$

$$k = 2,\ \gamma_o r_2 + \gamma_1 r_1 + \gamma_2 r_o + \ldots + \gamma_N r_{N-2} = 0 \qquad \text{(A8)}$$

$$k = N,\ \gamma_o r_N + \gamma_1 r_{N-1} + \gamma_2 r_{N-2} + \ldots \gamma_N r_o = 0$$

An additional equation which defines E_N results for k = 0 when Eq. (A6) is evaluated as follows:

$$E_N = \gamma_o \sum_{n=o}^{N} \gamma_n r_n \qquad \text{for } k = o \qquad \text{(A9)}$$

where it is recalled that $\gamma_o = 1$.

Burg (1967) has assumed that the mean squared error power E_N, as defined by Eq. (A5) for the time domain, is equivalent to the mean squared error power P_N, which is given by Eq. (8) for the frequency domain. However, King (1977) has noted that E_N and P_N are equivalent only when the predicted noise power equals the actual noise power or when the noise power is negligible. It follows that for high signal-to-noise conditions, it may be assumed that

$$P_N = E_N \qquad \text{(A10)}$$

and P_N may be evaluated as follows:

$$k = o,\ P_N = \sum_{n=o}^{N} \gamma_n r_n \qquad \text{(A11)}$$

or

$$\gamma_o r_o + \gamma_1 r_1 + \gamma_2 r_2 + \cdots \gamma_N r_N = P_N \tag{A12}$$

If Eq. (A12) is combined with the set of equations, Eq. (A8), the resulting set of equations may be expressed in matrix formulation as follows:

$$\begin{bmatrix} r_o & r_1 & r_2 & r_3 & \cdots & r_N \\ r_1 & r_o & r_1 & r_2 & \cdots & r_{N-1} \\ r_2 & r_1 & r_o & r_1 & \cdots & r_{N-2} \\ \cdot & & & & & \\ \cdot & & & & & \\ \cdot & & & & & \\ r_N & r_{N-1} & r_{N-2} & r_{N-3} & \cdots & r_o \end{bmatrix} \begin{bmatrix} \gamma_o \\ \gamma_1 \\ \gamma_2 \\ \cdot \\ \cdot \\ \cdot \\ \gamma_N \end{bmatrix} = \begin{bmatrix} P_N \\ 0 \\ 0 \\ \cdot \\ \cdot \\ \cdot \\ 0 \end{bmatrix} \tag{A13}$$

APPENDIX B

Burg (1968) has proposed a method for computing a set of N+1 prediction error filter coefficients as a function of a known set of N coefficients using the Levinson recursion equation that follows:

$$\gamma_k^{N+1} = \gamma_k^N + \gamma_{N+1}^{N+1}\,\gamma_{N-k+2}^N \tag{B1}$$

where the only unknown in Eq. (B1) is the last coefficient γ_{N+1}^{N+1} of the new set. Burg suggested that the unknown coefficient γ_{N+1}^{N+1} be obtained in a least square error analysis that incorporates both the forward and backward prediction of the k^{th} point as follows:

$$\vec{X}_k = \sum_{n=1}^{N} a_n^N\, x_{k-n} \tag{B2}$$

$$\overleftarrow{X}_k = \sum_{n=1}^{N} a_n^N\, x_{k+n} \tag{B3}$$

where the forward prediction $\vec{X}_k$ and the backward prediction $\overleftarrow{X}_k$ are expressed as discrete convolutions of the prediction filter set a_n^N (of size N) with the set of N+1 data samples. Both filters are illustrated in Fig. (3).

It follows that corresponding forward and backward prediction errors, denoted by α_k^N and β_k^N respectively, have the following representations.

$$\alpha_k^N = X_k - \vec{X}_k$$

$$\alpha_k^N = \sum_{n=0}^{N} \gamma_n^N\, x_{k-n} \qquad \text{for } N+1 \leq k \leq M \tag{B4}$$

$$\beta_k = X_k - \overleftarrow{X}_k \qquad \text{for } 1 \leq k \leq M-N \tag{B5}$$

$$\beta_k^N = \sum_{n=0}^{N} \gamma_n^N \, x_{k+n}$$

where $\gamma_1^{N+1} = 1$ and $\gamma_n^N = -a_n^N$.

Barnard (1975) has noted that the forward and backward prediction errors are interrelated through the Levinson recursion relations that follow.

$$\alpha_k^{N+1} = \gamma_{N+1}^{N+1} \cdot \beta_{k-N}^N + \alpha_k^N \,, \quad (N+1 \leq k \leq M) \tag{B6}$$

$$\beta_j^{N+1} = \gamma_{N+1}^{N+1} \cdot \alpha_{j+N}^N + \beta_j^N \,, \quad (1 \leq j \leq M-N) \tag{B7}$$

The prediction errors may be computed with the Levinson recursion relations, given by Eqs. (B6) and (B7), in a bootstrap manner that greatly reduces the number of computations required with use of the matrix formulation given by Eq. (10).

The total mean squared error may be expressed as the sum of the forward and backward mean squared errors as follows:

$$E_N = \frac{1}{2(M-N)} \sum_{k=1}^{M-N} \left[\left(\alpha_{k+N}^N \right)^2 + \left(\beta_k^N \right)^2 \right] \tag{B8}$$

for a filter of size N where $N \leq M-1$, M = number data samples.

In order to utilize Eqs. (B6) and (B7) as written, the total mean squared error may be expressed for filter size N+1 as follows:

$$E_{N+1} = \frac{1}{2(M-N-1)} \sum_{k=1}^{M-N-1} \left[\left(\alpha_{k+N+1}^{N+1} \right)^2 + \left(\beta_k^{N+1} \right)^2 \right] \tag{B9}$$

REFERENCES

1. Akaike, H., 1974 "A New Look at the Statistical Model Identification," IEEE Trans.Automat. Control, AC-19, pp. 716-723.

2. Anderson, Nils O., Feb 1974, "On the Calculation of Filter Coefficients for Maximum Entropy Spectral Analysis," Geophysics, Vol. 39. No. 1. pp. 69-72.

3. Barnard, Thomas E., June 1975, "The Maximum Entropy Spectrum and the Burg Technique," ALEX (03)-TR-75-01, Texas Instruments, Inc., Equipment Group, P.O. Box 6015, Dallas, Texas.

4. Blizard Marvin, ONR Code 222, Arlington, VA - private communication.

5. Burg, John P., Oct. 1967, "Maximum Entropy Spectral Analysis," presented at the 37th Meeting of the Society of Exploration Geophysicists, Oklahoma City, Oklahoma.

6. Burg, John P., 1968, "A New Analysis Technique for Time Series Data," presented at the NATO Advanced Study Institute on Signal Processing with Emphasis on Underwater Acoustics, Enschede, Netherlands.

7. Capon, J., 1969, "High-Resolution Frequency-Wavenumber Spectrum Analysis," Proc. IEEE, Vol. 57, pp. 1408-1418.

8. Chen and Stegen, July 1974, "Experiments with Maximum Entropy Power Spectra of Sinusoids," Jour. of Geophysical Research, Vol. 79, No. 20, pp. 3019-3022.

9. Fougere, Zawalick and Radoski, 1976, "Spontaneous Line Splitting in Maximum Entropy Power Spectrum Analysis," Physics of the Earth and Planetary Interiors, Vol. 12, pp. 709-720.

10. Gerchburg, R.W., 1974, "Super Resolution through Error Energy Reduction," Optica Acta, Vol. 21, No. 9, pp. 709-720.

11. Gray, May, 1977, "G-Spectral Estimation," IEEE-International Conference on Acoustic Speech and Signal Processing, Hartford, Connecticut.

12. Kaveh and Cooper, May 1976, "An Empirical Investigation of the Properties of the Autoregressive Spectral Estimator," IEEE Transactions on Information Theory," Vol. II-22, No. 3, pp. 313-323.

13. King, William R., Nov. 1977, "Some Effects of Noise Upon Maximum Entropy Spectral Analysis," NRL Memo Rpt. 3645, Naval Research Laboratory, Washington, D.C.

14. Lacoss, Richard T., Aug. 1971, "Data Adaptive Spectral Analysis Methods," Geophysics, Vol. 36, No. 4, pp. 661-675.

15. Levinson, H. ,1947. "The Wiener RMS Error Criterion in Filter Design and Prediction," J. Math. Phys., Vol. 25, pp. 261-278.

14. Lacoss, Richard T., Aug. 1071, "Data Adaptive Spectral Analysis Methods," Geophysics, Vol. 36, No. 4, pp. 661-675.

15. Levinson, H., 1947," The Wiener RMS Error Criterion in Filter Design and Prediction," J. Math. Phys., Vol. 25, pp. 261-278.

16. Nuttall, A.H., March 1976, "Spectral Analysis of a Univariate Process with Bad Data Points, via Maximum Entropy and Linear Predictive Techniques," NUSC Tech. Rept. 5303, Naval Underwater Systems Center, New London, Connecticut.

17. Papoulis, Sept., 1975, "A New Algorithm in Spectral Analysis and Band Limited Extrapolation," IEEE Trans. on Circuits and Systems, CAS-22, No. 9, pp. 735-742.

18. Parzen, E., 1969, "Multiple Time Series Modeling," in Multivariate Analysis-II, edited by P.R. Kirshnaiah, pp. 389-409, Academic Press, New York.

19. Ulrych and Bishop, 1975, "Maximum Entropy Spectral Analysis and Autoregressive Decomposition," Reviews of Geophysics and Space Physics, Vol. 13, No. 1, pp. 183-199.

20. Ulrych and Clayton, Jan. 1976, "Time Series Modeling and Maximum Entropy," Physics of the Earth and Planetary Interiors," 12, pp. 188-200.

21. Van den Bos, A., 1971, "Alternative Interpretation of Maximum Entropy Spectral Analysis," IEEE Trans. on Information Theory, IT-17, pp. 493-494.

22. Walker, G., 1931, "On Periodicity in Series of Related Terms," Proc. Roy. Soc., London, Ser. A, 131, pp. 518-532.

23. Yule, G.U., 1927, "On a Method of Investigating Periodicities in Disturbed Series with Special Reference to Wolfers Sunspot Numbers," Phil. Trans. Roy. Soc. London, Ser. A, 226, pp. 267-298.